Supporting Information

Biophysical techniques to distinguish ligand binding modes in cytochrome P450 monooxygenases

Matthew N. Podgorski,[†,⊥] Joshua S. Harbort,[‡,⊥] Tom Coleman, [†,⊥] Jeanette E. Stok,[¶] Jake A. Yorke,[∫] Luet-Lok Wong,[∫] John B. Bruning,[Δ] Paul V. Bernhardt,*[,¶] James J. De Voss, *[,¶] Jeffrey R. Harmer*[,‡] and Stephen G. Bell*[,†]

[†] Department of Chemistry, University of Adelaide, Adelaide, SA, 5005, Australia.

[‡] Center for Advanced Imaging, University of Queensland, St Lucia, Qld, 4072, Australia.

[¶] School of Chemistry and Molecular Bioscience, University of Queensland, St Lucia, Qld, 4072, Australia.

[∫] Department of Chemistry, University of Oxford, Inorganic Chemistry Laboratory, South Parks Road, Oxford, OX1 3QR, UK.

[Δ]School of Biological Sciences, University of Adelaide, SA 5005, Australia

Corresponding Authors

* stephen.bell@adelaide.edu.au
* jeffrey.harmer@cai.uq.edu.au
* j.devoss@uq.edu.au
* p.bernhardt@uq.edu.au

Contents

Experimental Section

General

General reagents, organic substrates were from Sigma-Aldrich, TCI, Fluorochem or VWR. Buffer components, NADH and isopropyl-β-D-thiogalactopyranoside (IPTG) were from Astral Scientific, Australia. The expression, purification and characterization of WT CYP199A4, HaPux and HaPuR were performed as described elsewhere.[1-3] The CYP199A4 protein concentration was calculated using ε_{419} = 119 mM^{-1} cm^{-1} as described previously.[1, 2]

Substrate binding: spin state determination and binding titrations

UV-vis spectra and spectroscopic activity assays were recorded at 30 ± 0.5 °C on an Agilent CARY-60 spectrophotometer. The high-spin heme content was determined using an enzyme concentration of 1.2-9.2 µM in 50 mM Tris, pH 7.4, with the addition of 0.5-1 µL aliquots of substrate (from a 100 mM stock) until the spectrum did not change. The percentage shift was estimated (to approximately ±5%) by comparison with a set of spectra generated from the sum of the appropriate percentages of the spectra of the substrate-free (>95% low-spin, Soret maximum at 418 nm) and camphor-bound (>95% high-spin, Soret maximum at 392 nm) forms of WT CYP101A1 as described previously.[4, 5] Chemical reduction experiments or those with the redox partners are described in the supporting information.

For dissociation constant determination CYP199A4 was diluted to 0.8 – 1.9 µM in 50 mM Tris, pH 7.4, in a total volume of 2.5 mL. Aliquots of the substrate (0.5-2 µL) were added using a Hamilton syringe from a 1, 10 or 100 mM stock solution in ethanol or DMSO. The maximum Soret band peak-to-trough difference (ΔA) in absorbance was recorded between 700 nm and 250 nm. Further aliquots of substrate were added until the peak-to-trough difference of the Soret band did not change. The dissociation constants, K_d, were obtained by fitting ΔA against total substrate concentration [S] to the tight binding quadratic equation:[6]

$$\frac{\Delta A}{\Delta A_{\max}} = \frac{([E]+[S]+K_d) - \sqrt{\{([E]+[S]+K_d)^2 - 4[E][S]\}}}{2[E]}$$

$\Delta A_{\max}$ is the maximum absorbance difference and [E] is the enzyme concentration.

Activity assays

In vitro NADH turnover rate assays were performed with mixtures (1.2 mL) containing 50 mM Tris, pH 7.4, 0.5 µM CYP199A4, 5 µM HaPux and 0.5 µM HaPuR. The buffer solution was oxygenated before addition of the enzymes and the mixtures equilibrated at 30 °C for 2 min. Substrates were added as a 100 mM stock solution in ethanol (4-methoxybenzoic acid) or DMSO (pyridinyl benzoic acids) to a final concentration of 1 mM. NADH was added to *ca*. 320 µM (final A_{340} = 2.00). The rate of NADH oxidation was calculated by monitoring the absorbance at 340 nm and using ε_{340} = 6.22 $mM^{-1}cm^{-1}$.

The concentration of hydrogen peroxide generated during the NADH turnovers was determined using a horseradish peroxidase (HRP)/phenol/4-aminoantipyrine (4-AP) assay.[7] The turnover incubation (400 µL) was mixed with 200 µL of 50 mM phenol (pH 7.4, Tris buffer) and 200 µL of 5 mM 4-AP (pH 7.4, Tris buffer). The absorbance at 510 nm was set to zero, and 1 µL of a 20 mg mL^{-1} solution of HRP was added. The absorbance at 510 nm was then recorded and used to calculate the concentration of hydrogen peroxide (ε_{510} = 6580 M^{-1} cm^{-1}).

Analysis of metabolites

Analytical High Performance Liquid Chromatography (HPLC) was performed on an Agilent 1260 Infinity Pump equipped with an autoinjector connected using a Phenomenex Kinetex 5µm, XB-C18,

100 Å column (250 mm x 4.6 mm, 5 μm). A gradient between 20-95% acetonitrile in water (0.1% trifluoroacetic acid) at a flow rate of 1 mL min^{-1} over 30 minutes was used and the eluate was monitored at 254 nm.

.

Table S1 Extinction coefficients of ferric CYP199A4 in complex with 4-(pyridin-2-yl)- and ferric and ferrous CYP199A4 with 4-(pyridin-3-yl)-benzoic acid compared to the substrate-free (SF) ferric form. λ_{max} is reported in nm and the extinction coefficient (ε) in mM^{-1} cm^{-1}.

CYP199A4 Complex	δ		Soret band		β		α	
	λ_{max}	ε	λ_{max}	ε	λ_{max}	ε	λ_{max}	ε
Fe(III) SF	357	32.6	419	119 [8]	537	11.0	569	12.3
Fe(III) + 4-py2BA	359	31.6	422	115	540	11.3	571	13.6
Fe(III) + 4-py3BA	364	35.7	424	106	541	10.8	shoulder at ~570	8.4
Fe(II) + 4-py3BA	-	-	447	118	542	18.6	571	19.6

Determination of the extinction coefficients of ferric and ferrous forms of CYP199A4

Method details

The UV-Vis spectrum of 1000 µL of 7.1 µM WT CYP199A4 in 50 mM Tris-HCl buffer (pH 7.4) was recorded and the extinction coefficients of the α, β, and δ bands were determined. The literature Soret band extinction coefficient (ε_{419} = 119 mM^{-1} cm^{-1})[8] was used to determine P450 concentration. To form the complex of CYP199A4 with 4-(pyridin-3-yl)benzoic acid and 4-(pyridin-2-yl)benzoic acid, 20 µL of a 100 mM solution in DMSO was added to the cuvette. To generate the ferrous form, a few grains of sodium dithionite were added to the cuvette and the UV-Vis spectrum was recorded.

Extinction coefficients of native CYP199A4

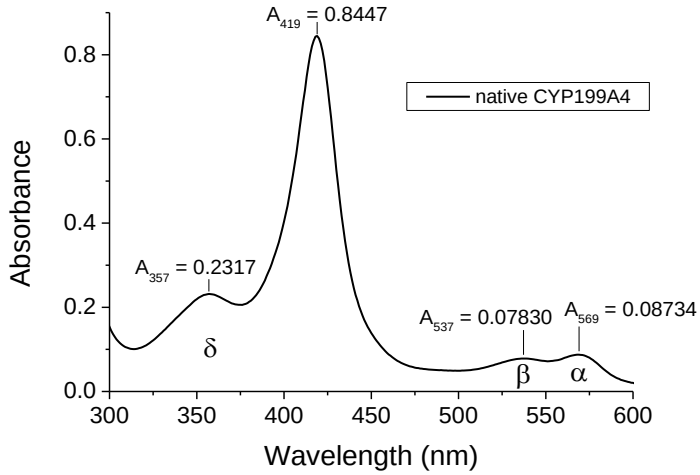

UV-Vis spectrum of ferric substrate-free WT CYP199A4.

The extinction coefficient of CYP199A4 reported in the literature is ε_{419} = **119 mM^{-1} cm^{-1}**.[8]

Concentration of P450 in cuvette: c = $A_{419}/\varepsilon_{419}$ = 0.845/119 mM^{-1} cm^{-1} = **7.10 µM**

Extinction coefficients of ferric CYP199A4 in complex with 4-(pyridin-3-yl)benzoic acid

To form the complex of CYP199A4 with 4-(pyridin-3-yl)benzoic acid, 20 µL of a 100 mM solution of 4-(pyridin-3-yl)benzoic acid in DMSO was added to the cuvette. The protein solution in the cuvette was therefore diluted from 1000 µL to 1020 µL. Hence, the protein concentration was reduced from 7.10 µM to 6.96 µM.

$c_i v_i = c_f v_f$

c_f = (1000 µL/1020 µL) × 7.098 µM = **6.96 µM**

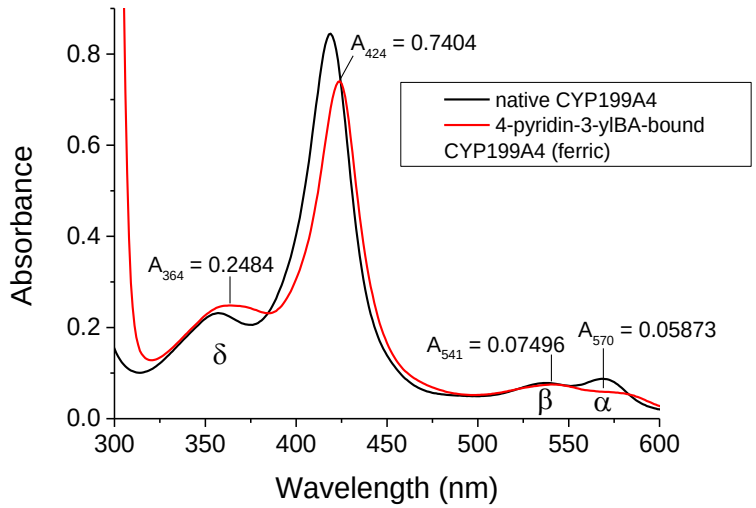

UV-Vis spectrum of ferric CYP199A4 in complex with 4-(pyridin-3-yl)benzoic acid (**red**).

Extinction coefficients of ferrous CYP199A4 in complex with 4-(pyridin-3-yl)benzoic acid

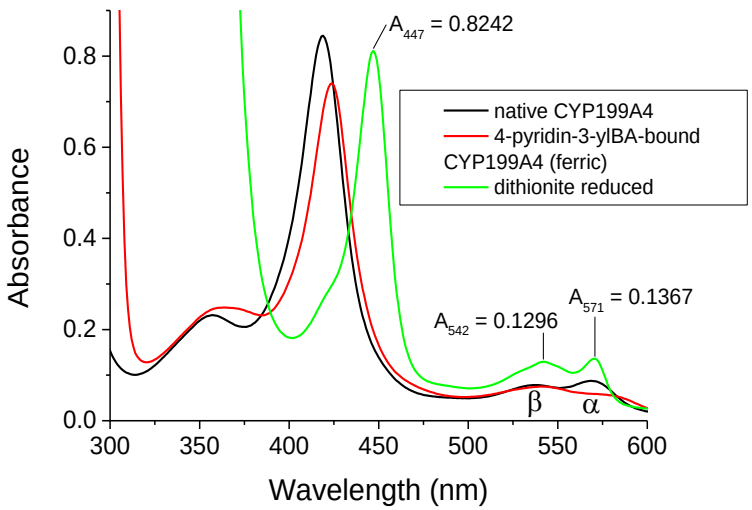

UV-Vis spectrum of ferrous CYP199A4 in complex with 4-(pyridin-3-yl)benzoic acid (**green**).

Extinction coefficients of ferric CYP199A4 in complex with 4-(pyridin-2-yl)benzoic acid

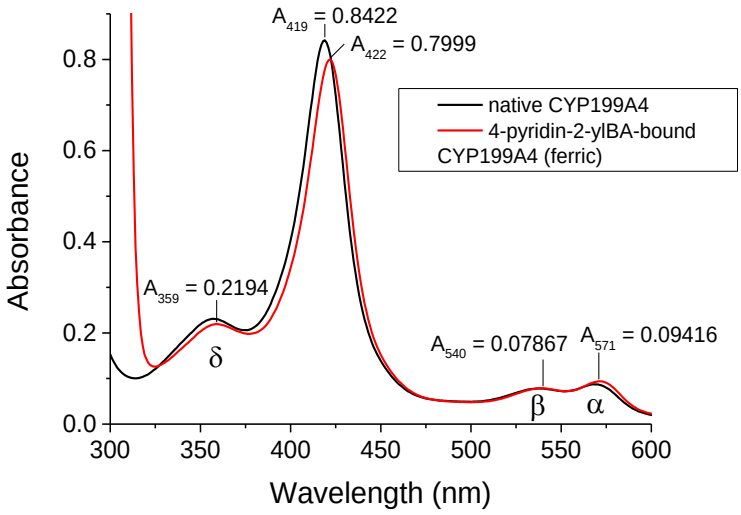

UV-Vis spectrum of ferric CYP199A4 in complex with 4-(pyridin-2-yl)benzoic acid (**red**).

Table S2 Spectroelectrochemically determined CYP199A4 optical spectra in its ferric and ferrous forms (~20 μM) in the absence and presence of substrates (~1 mM) at pH 7.4.

	Fe(III)	Fe(II)
No substrate	417, 546, 561 nm	414, 548 nm
4-methoxybenzoic acid	390, 500, 645 nm	412, 544 nm
4-(pyridin-2-yl)benzoic acid	420, 538, 567 nm	412, 544 nm
4-(pyridin-3-yl)benzoic acid	422, 532, 562 nm	447, 540, 567 nm

Table S3 Statistics for data collection and refinement of crystal structures of WT CYP199A4 in complex with type II ligands; 4-(pyridin-2-yl)benzoic acid and 4-(pyridin-3-yl)benzoic acid (BA benzoic acid). Values in parentheses correspond to the highest resolution (outer) shell.

Statistic	4-(pyridin-2-yl)-BA	4-(pyridin-3-yl)-BA
PDB code	6U3K	6U30
X-ray wavelength (Å)	0.9537	0.9537
Unit cell parameters (Å/°)	a = 44.3 b = 51.2 c = 79.2 α = 90.0 β = 92.4 γ = 90.0	a = 44.4 b = 51.5 c = 78.8 α = 90.0 β = 92.1 γ = 90.0
Space group	$P12_11$	$P12_11$
Molecules per asymmetric unit	1	1
Resolution range	44.23 – 1.80 (1.84 – 1.80)	44.36 – 1.66 (1.68 – 1.66)
<I/σ(I)>	3.0 (0.9)	14.2 (3.4)
Unique reflections	32441	42402
Completeness of data	98.3 (97.1)	99.7 (96.7)
Multiplicity	7.2 (7.3)	7.0 (6.0)
R_{merge} (all I+ and I−)	49.2 (280.7)	9.3 (48.9)
R_{pim} (all I+ and I−)	19.6 (109.9)	3.8 (21.5)
$CC_{1/2}$	93.4 (44.6)	99.8 (90.7)
R_{work}	0.197	0.151
R_{free} (5% held)	0.241	0.192
Ramachandran favored (%)	97.95	98.47
Ramachandran outliers (%)	0	0
Unusual rotamers (%)	0.31	0.62
r.m.s.d. bond angles (°)	0.795	1.02
r.m.s.d. bond lengths (Å)	0.006	0.009
Omit map type, contour level, carve radius	feature-enhanced map, 1.5 σ, 1.5 Å carve	composite omit map, 1.5 σ, 1.2 Å carve

Table S4 Distances (in angstroms) of key structural features of 4-(pyridin-3-yl)benzoic acid- and 4-(pyridin-2-yl)benzoic acid-bound CYP199A4.

Distance (Å)	**4-(pyridin-3-yl)-BA**	**Distance (Å)**	**4-(pyridin-2-yl)-BA**
Fe - N	2.2	Fe - W1 (aqua ligand to heme)	2.2
Fe - C_{04}	3.0	Fe - N	4.2
Fe - C_{06}	3.1	N - W1	2.9
C_{02} - closest F298 C	3.6	C_{01}- closest F298 C	3.8
C_{02} - closest F185 C	4.8	C_{02} - closest F185 C	3.7
C_{02} - closest F182 C	3.4	C_{02} - closest F182 C	3.6
N - closest T252 C	3.7	Fe - C_{05}	4.4
N - closest F182 C	5.0	N - closest F182 C	3.6
O_{15} - W1 (bridging water)	2.5	O_{15} - W10 (bridging water)	2.6
O_{15} - closest R92 N	2.9	O_{15} - closest R92 N	3.0
C_7 - closest A248 C	3.4	C_5 - W1	3.3
C_7 - closest L98 C	4.1	C_7 - closest L98 C	3.7
Angle (°)		**Angle (°)**	
(C358)S-Fe-N(pyridine)	176.9	(C358)S-Fe-(W1)	163.4
Dihedral C_{04}-C_{03}-C_{07}-C_{08}	40.21	Dihedral N-C_{03}-C_{07}-C_{08}	60.62
Refined occupancy (%)		**Refined occupancy (%)**	
4-(pyridin-3-yl)benzoic acid ligand	99	4-(pyridin-2-yl)benzoic acid ligand	100
		W1 (aqua ligand to heme)	76

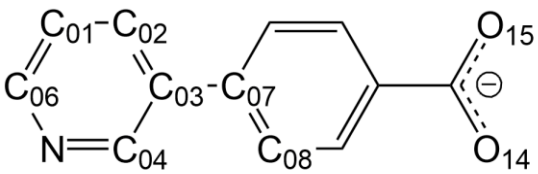

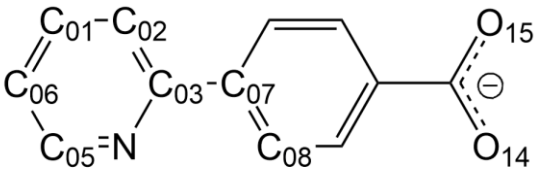

Table S5 Distances between equivalent atoms of 4-(pyridin-3-yl)benzoic acid (4Py3BA) and 4-(pyridin-2-yl)benzoic acid (4Py2BA) and displacement of nearby active-site residues. The nomenclature used to specify the position of atoms in the amino acid residues is that described by Markley *et al.*[9]

Distances between equivalent atoms of 4Py2BA and 4Py3BA (Å)	
C_1 - C_1	3.1
C_2 - C_2	2.3
C_3 - C_3	1.7
C_4 - N_4	2.1
N_5 - C_5	2.7
C_6 - C_6	3.1
C_7 - C_7	1.2
C_8 - C_8	0.9
C_9 - C_9	0.6
C_{10} - C_{10}	0.4
C_{11} - C_{11}	0.6
C_{12} - C_{12}	1.0
C_{13} - C_{13}	0.3
O_{14} - O_{14}	0.3
O_{15} - O_{15}	0.4

Displacement of F182 phenyl ring (Å)	
C^{γ}	0.8
$C^{\delta1}$	0.9
$C^{\varepsilon1}$	0.9
C^{ζ}	0.9
$C^{\varepsilon2}$	0.9
$C^{\delta2}$	0.8

Displacement of F298 phenyl ring (Å)	
C^{γ}	1.1
$C^{\delta1}$	2.9
$C^{\varepsilon1}$	4.7
C^{ζ}	4.4
$C^{\varepsilon2}$	2.4
$C^{\delta2}$	1.4

Displacement of F185 phenyl ring (Å)	
C^{γ}	0.4
$C^{\delta1}$	0.4
$C^{\varepsilon1}$	0.5
C^{ζ}	0.4
$C^{\varepsilon2}$	0.5
$C^{\delta2}$	0.5

Displacement of bridging water (Å)	
W1 - W10	0.3

Displacement of V295 (Å)	
C^{β}	1.1
$C^{\gamma1}$	1.3
$C^{\gamma2}$	1.1

Displacement of A248 (Å)	
C^{α}	0.8
C^{β}	1.0

Displacement of T252 (Å)	
C^{β}	0.9
$C^{\gamma2}$	1.0
$O^{\gamma1}$	0.9

Displacement of V181 (Å)	
C^{β}	0.4
$C^{\gamma1}$	0.4
$C^{\gamma2}$	0.3

Displacement of L98 (Å)	
C^{γ}	0.4
$C^{\delta1}$	0.5
$C^{\delta2}$	0.6

4Py3BA

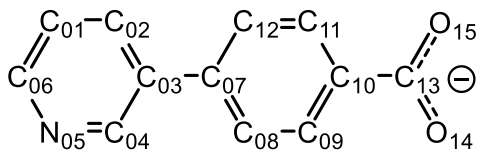

4Py2BA

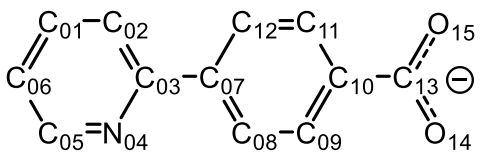

Table S6 Fe-N (pyridine) bond distances in crystal structures of P450 enzymes with directly coordinated pyridine derivatives

PDB code	Description	Fe-N (pyridine) distance (Å)	Angle between pyridine ring and Fe-S bond (˚)	Angle between pyridine ring and the heme plane (˚)
4I4H[10]	Crystal structure of CYP3A4 ligated to pyridine-substituted desoxyritonavir	2.14	2.0	84.3
3QU8[11]	Crystal structure of a human cytochrome P450 2B6 (Y226H/K262R) in complex with the inhibitor 4-(4-nitrobenzyl)pyridine	2.37, 2.28, 2.25, 2.34, 2.30	6.6	82.9
1W0G[12]	Crystal structure of metyrapone-bound human cytochrome P450 3A4	2.27	12.9	72.1
3QOA[11]	Crystal structure of a human cytochrome P450 2B6 (Y226H/K262R) in complex with the inhibitor 4-benzylpyridine	2.36	9.4	89.3
1PHG[13]	Crystal Structure of Metyrapone-Inhibited Complex of Cytochrome P450-CAM	2.16	5.1	80.1

The Fe-N(pyridine) bond length in the 4-(pyridin-3-yl)benzoic acid-bound $WT_{CYP199A4}$ crystal structure was refined to 2.2 Å. This bond length is longer than the Fe-N(pyridine) bond length in $[Fe(bpy)_3]^{2+}$, which is 1.97 Å (bpy; bipyridine).[14] However, it is comparable to the Fe-N(pyridine) bond lengths in crystal structures of other P450s with directly bound pyridine derivatives in the PDB (~2.1 – 2.4 Å).[10-13]

The heme plane was defined by the four heme pyrrole N.

Table S7 CW EPR parameters for CYP199A4 with various substrates determined from spectrum simulation. Spectra are modeled as a sum of separate LS and HS EPR components. Error in the *g*-values determination is ±0.0010.

Substrate	component	Spin State	Comp. %	g_z	g_y	g_x	g_z *strain*	g_y *strain*	g_x *strain*	*D*	*E/D*
Substrate-free	*1*	LS	100	2.4332	2.2530	1.9141	0.0308	0.0182	0.0179		
4-MeOBA	*1*	LS	50.4	2.4147	2.2549	1.9216	0.0262	0.0170	0.0151		
	2	″	21.1	2.4546	2.2561	1.9039	0.0418	0.0195	0.0208		
	3	″	8.5	2.3851	2.2366	1.9811	0.0279	0.0183	0.0102		
	4 [a]	HS	20.0	8.0990	3.4808	1.6695	0.2337	0.1650	0.0633	~10^8 [c]	~0.108 [c]
4Py2BA	*1*	LS	100	2.4388	2.2504	1.9103	0.0246	0.0117	0.0117		
4Py3BA	*1*	LS	94.4	2.5262	2.2583	1.8798	0.0385	0.0156	0.0201		
	2 [b]	″	5.6	2.4112	2.2665	1.9195	0.0299	0.0079	0.0120		

[a] Modeled with an S_{eff} = 1/2 spin Hamiltonian. [b] Assigned to signal from remaining CYP199A4 not directly coordinating 4Py3BA. [c] Modeled with a spin Hamiltonian with an S = 5/2 spin, g = 2 and the D and E/D values listed.

4-Methoxybenzoic acid (4MeOBA), 4-(pyridin-2-yl)benzoic acid (4Py2BA), and 4-(pyridin-3-yl)benzoic acid (4Py3BA).

Table S8 Displacement of the iron below the porphyrin plane in CYP199A4 crystal structures (all distance are in angstroms).

Ligand bound to wild-type CYP199A4		Iron displacement below porphyrin plane	
		Plane as defined by the four pyrrole nitrogens	Plane as defined by the 24 atoms of the porphyrin macrocycle
4-(Pyridin-3-yl)BA	6 coordinate, low-spin	0.053 Å	0.042 Å
4-(Pyridin-2-yl)BA		0.13 Å	0.10 Å
4-MethylBA (6PQS)	5-coordinated high-spin	0.31 Å	0.29 Å
4-MethoxyBA (4DO1)		0.20 Å	0.23 Å
4-EthoxyBA (5U6T)		0.28 Å	0.26 Å

Table S9 Iron-sulfur bond distances in CYP199A4 crystal structures

Ligand bound to wild-type CYP199A4		Iron-sulfur bond length (Å)
4-(Pyridin-3-yl)BA	6 coordinate, low-spin	2.30
4-(Pyridin-2-yl)BA		2.29
4-MethylBA (6PQS)	5-coordinated high-spin	2.34
4-MethoxyBA (4DO1)		2.40
4-EthoxyBA (5U6T)		2.40

Table S10 Fe-N(porphyrin) bond distances in CYP199A4 crystal structures

WT CYP199A4 crystal structure	Fe-N_A	Fe-N_B	Fe-N_C	Fe-N_D
4-(Pyridin-3-yl)BA	2.05	2.04	2.04	2.05
4-(Pyridin-2-yl)BA	2.02	2.08	2.05	2.04
4-MethylBA (6PQS)	2.06	2.06	2.05	2.05
4-MethoxyBA (4DO1)	2.13	2.03	2.07	2.13
4-EthoxyBA (5U6T)	2.05	2.05	2.10	2.11

Figure S1 UV-Vis spectra of CYP199A4 in complex with 4-(pyridin-3-yl)benzoic acid (red) and 4-(pyridin-2-yl)benzoic acid (blue). In black is substrate-free CYP199A4.

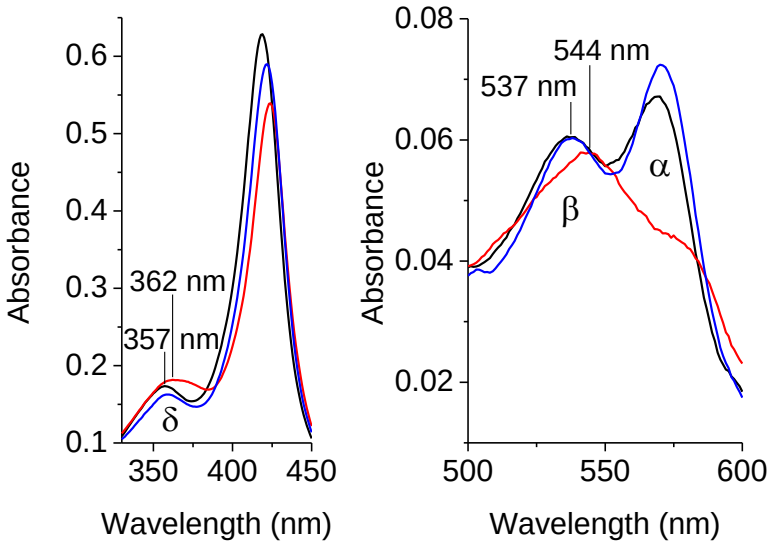

Binding of 4-(pyridin-3-yl)benzoic acid substantially reduces the intensity of the α-band and the β-band is red-shifted by ~7 nm. This ligand would be classified as a 'normal' nitrogen donor ligand.[15] The band at 357 nm is also red-shifted and the intensity increased.

In contrast, for 4-(pyridin-2-yl)benzoic acid-bound CYP199A4 the α-band is more intense than the β-band. This part of the spectrum is similar to the spectra described by Dawson and Sono for certain 'abnormal' nitrogen donor ligands.[15] For both complexes, the intensity of the β-band is similar.

Figure S2 The dissociation constant assays of CYP199A4 with (a) 4-(pyridin-2-yl)- and (b) 4-(pyridin-3-yl)benzoic acid. The concentration of the enzyme used in the dissociation constant assays above were 4.3 and 2.6 μM, respectively.

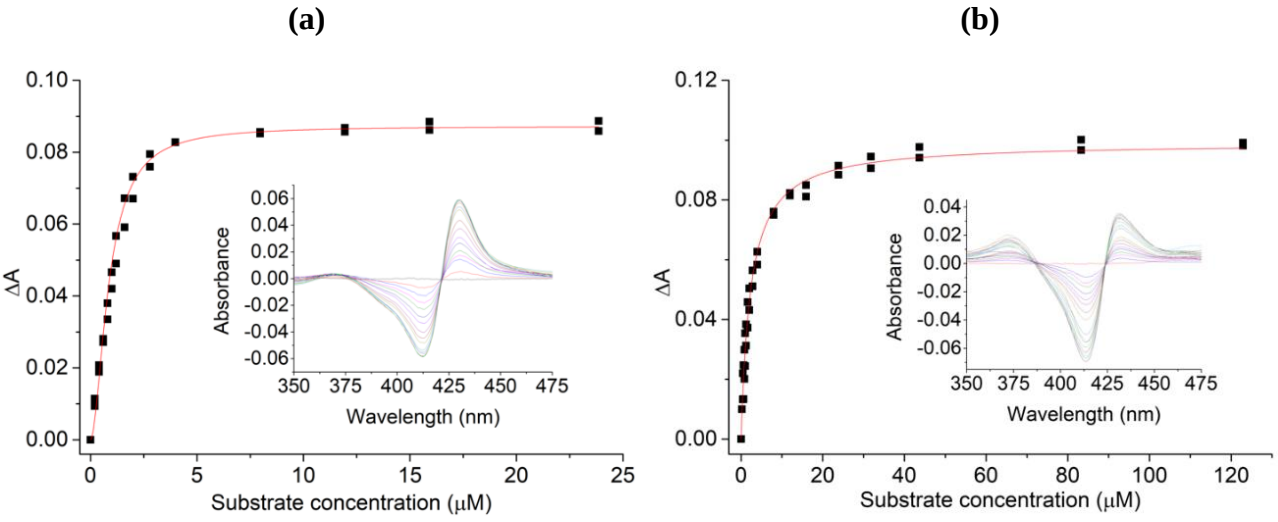

Figure S3 Mediators used in optical spectroelectrochemistry experiments and their $Co^{III/II}$ redox potentials at pH 7 (versus NHE).

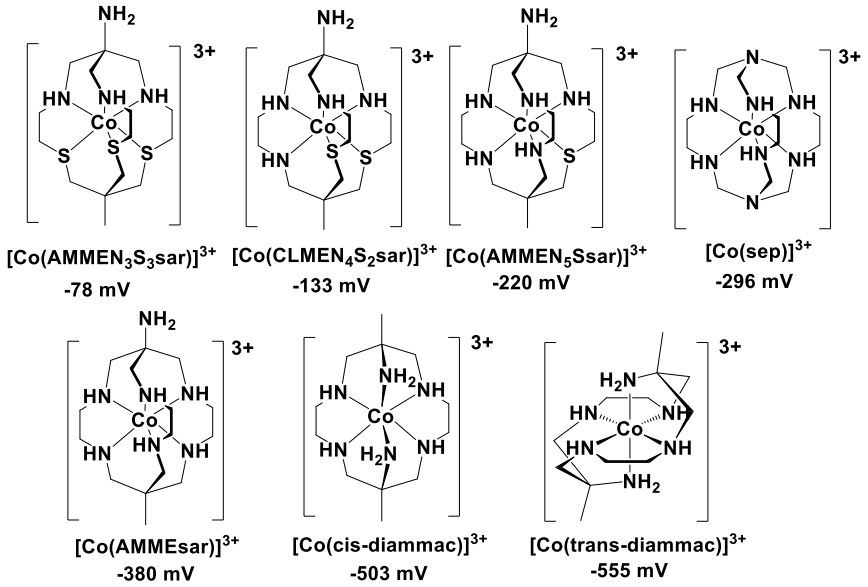

Figure S4 The calculated spectra, the draw data and the fit at a single wavelength for the reduction potential measurements of CYP199A4 bound to different substrates and the substrate-free form.

(a) Substrate-free CYP199A4

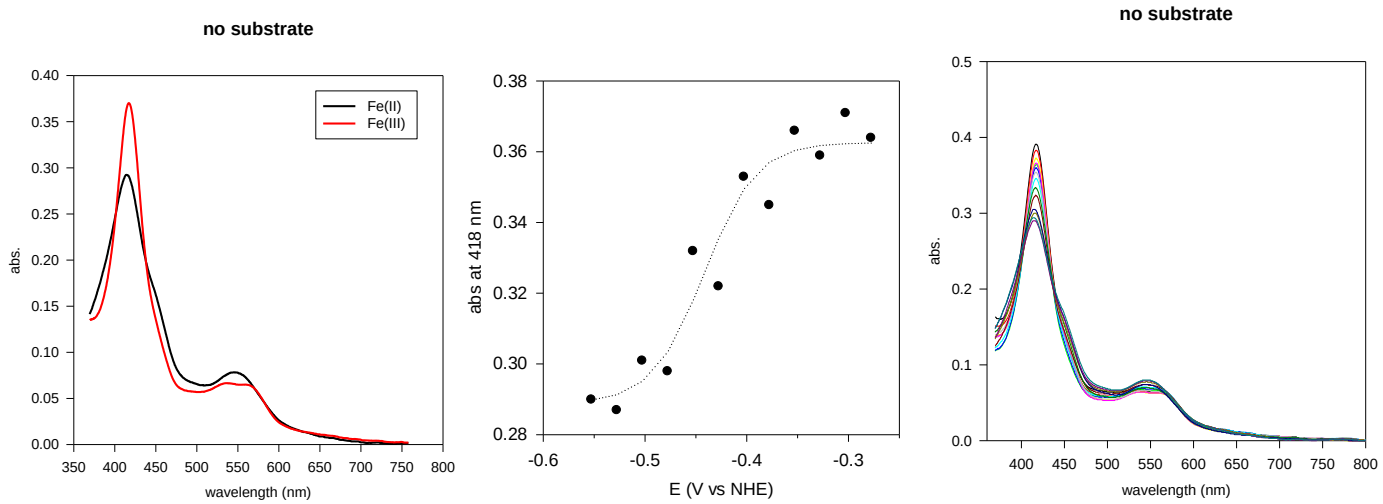

(b) 4-methoxybenzoic acid bound CYP199A4

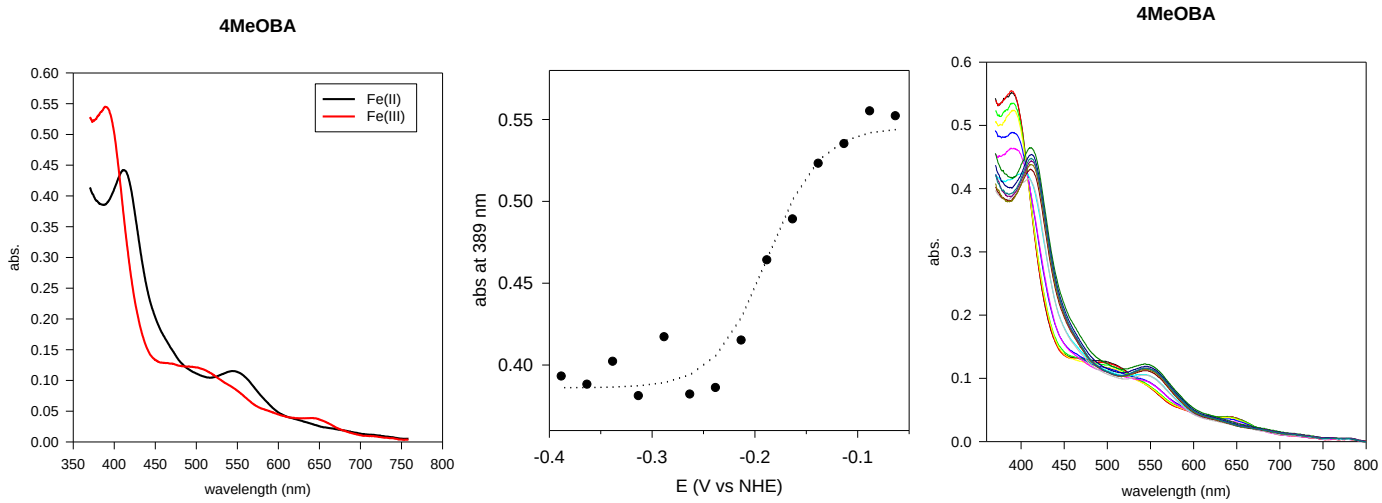

(c) 4-(pyridin-2-yl)benzoic acid bound CYP199A4

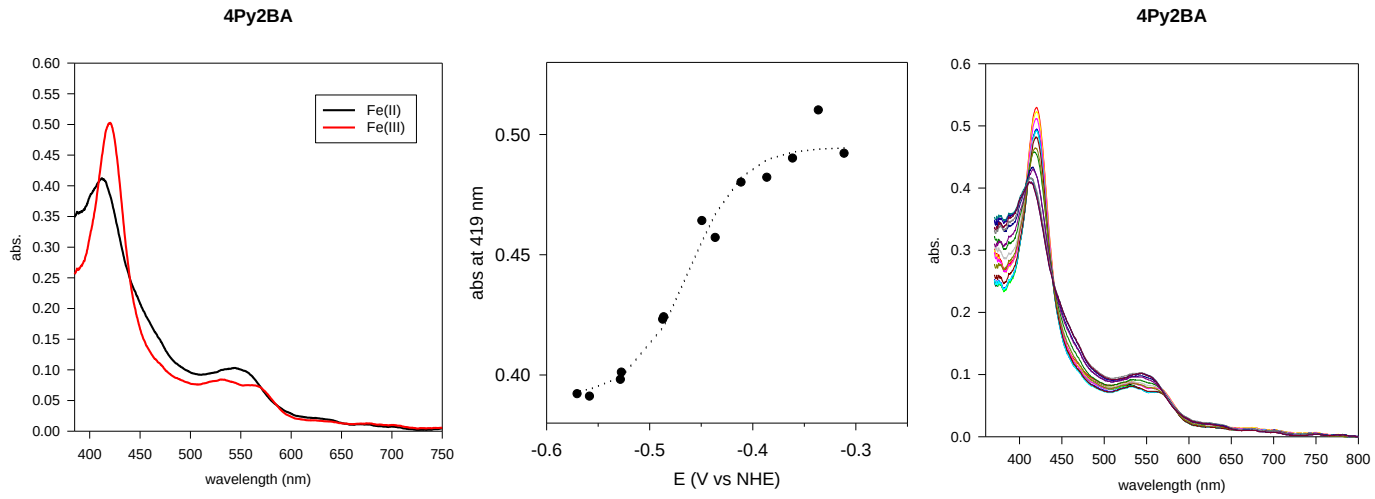

(d) 4-(pyridin-3-yl)benzoic acid bound CYP199A4

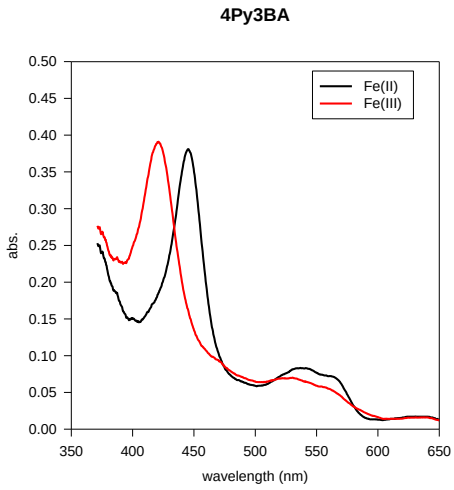

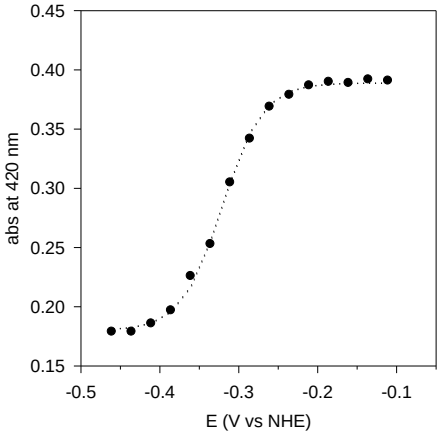

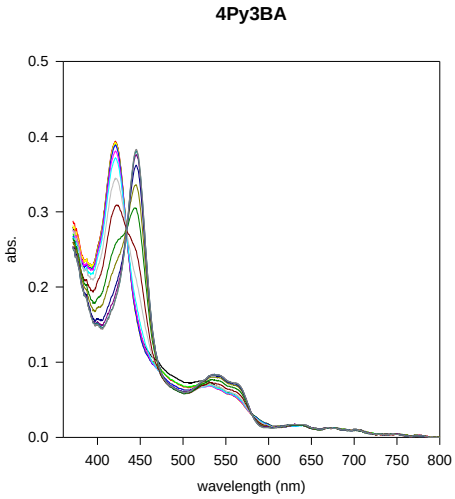

Figure S5 Potentiometric titrations for substrate-free CYP199A4 (left) and 4-methoxybenzoic acid-bound CYP199A4 (right) using organic mediators. The inset shows a non-linear least-squares fit of absorbance at 465 nm to a sigmoidal form of the Nernst equation with the number of electrons fixed at 1. The reduction potentials were determined to be –461 ± 6 mV (substrate-free) and –218 ± 3 mV (substrate-bound) a shift of ΔE = +243 mV under these conditions.

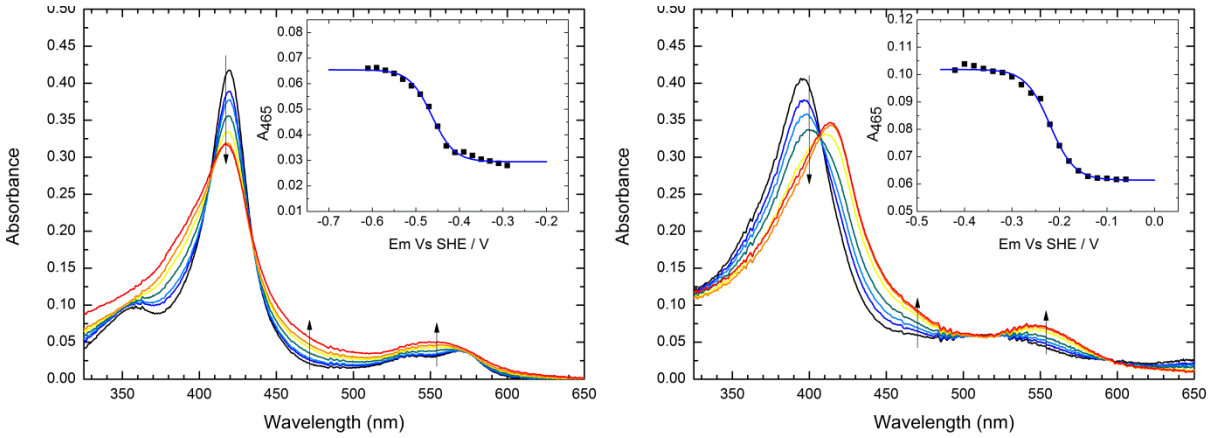

Figure S6 UV-Vis spectra of ferrous WT CYP199A4 in complex with substrates and type II inhibitors; substrate-free (black), substrate-bound (red) and reduced substrate-bound (green). Shown are 4-methoxybenzoic acid (4MethoxyBA), and 4-(pyridin-2-yl)benzoic acid (4Py2BA). The ferrous and ferrous CO-bound spectra are shown below for comparison.

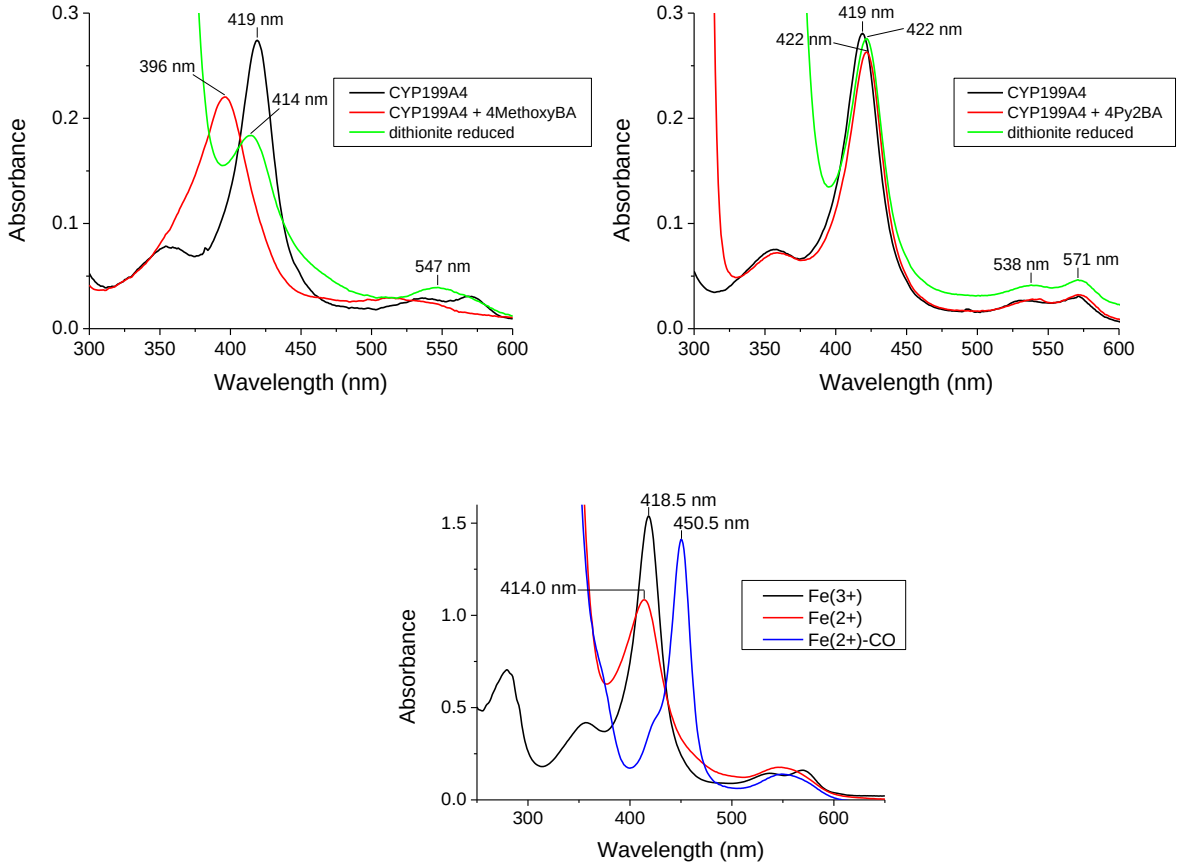

Method

The UV-Vis spectrum of 1 mL of CYP199A4 was recorded (pH 7.4, 50 mM Tris-HCl) and the protein was then saturated with substrate/inhibitor (≥1 mM). Sodium dithionite was added and the spectrum of the ferrous P450 complex was recorded.

Reduction of the complexes of CYP199A4 with 4-methoxybenzoic resulted in a spectrum with peaks at ~414 nm and ~547 nm. Reduction of the 4-(pyridin-3-yl)benzoic acid-CYP199A4 complex resulted in a shift of the Soret peak to 447 nm, with prominent peaks present at 541 and 571 nm. The spectrum of the ferrous CYP199A4-inhibitor complex indicates direct coordination of the pyridine moiety to the heme. This spectrum is consistent with the spectra reported by Dawson for ferrous $P450_{cam}$ in complex with σ-donor nitrogen ligands (metyrapone, pyridine and *N*-phenylimidazole) which were characterized by red-shifted Soret peaks around 440 nm.[16] Reduction of the 4-(pyridin-2-yl)benzoic acid-CYP199A4 complex did not shift the Soret band indicating that dithionite may not be able to reduce this CYP199A4 complex.

Figure S7 UV-Vis spectra of ferrous WT CYP199A4 in complex with pyridine and imidazole; substrate-free (black), substrate-bound (red) and reduced substrate-bound (green).

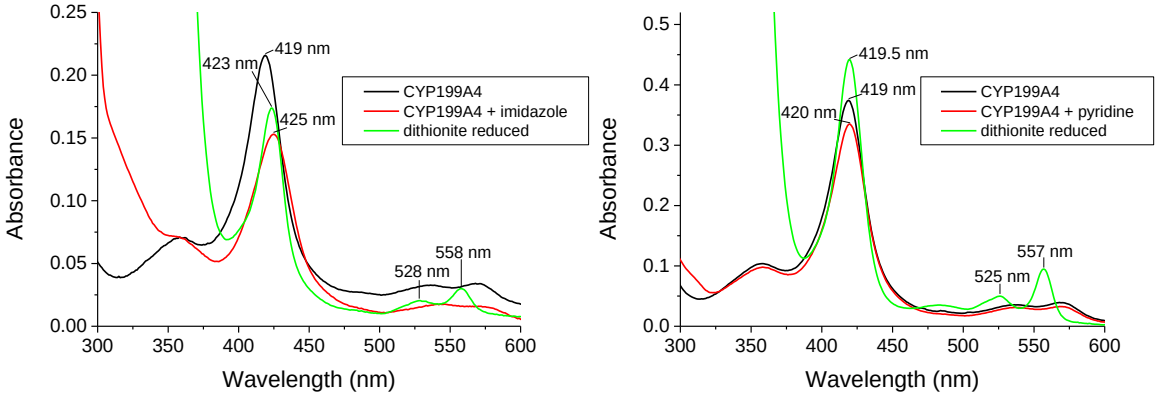

UV-Vis spectra were obtained of ferrous CYP199A4 in complex with imidazole and pyridine. The Soret peak failed to shift to ~447 when dithionite was added to the CYP199A4-ligand complexes.

The UV-Vis spectrum of 1 mL of WT CYP199A4 in 50 mM Tris-HCl buffer (pH 7.4) was recorded and the P450 was then complexed with imidazole (400 mM) or pyridine (370 mM). Dithionite was added to reduce the P450 and the UV-Vis spectrum of the ferrous CYP199A4-ligand complex was recorded. Upon reduction, spectral changes were observed; however, the Soret peak failed to shift to ~447 nm.

Figure S8 UV-Vis spectra of ferrous WT CYP199A4 in complex with type II inhibitors and substrates (addition of substrate after reduction); substrate-free (black), reduced substrate-free (red) and reduced substrate-bound (green). Shown are 4-methoxybenzoic acid (4MethoxyBA), 4-(pyridin-2-yl)benzoic acid (4Py2BA), 4-(pyridin-3-yl)benzoic acid (4Py3BA), pyridine and imidazole.

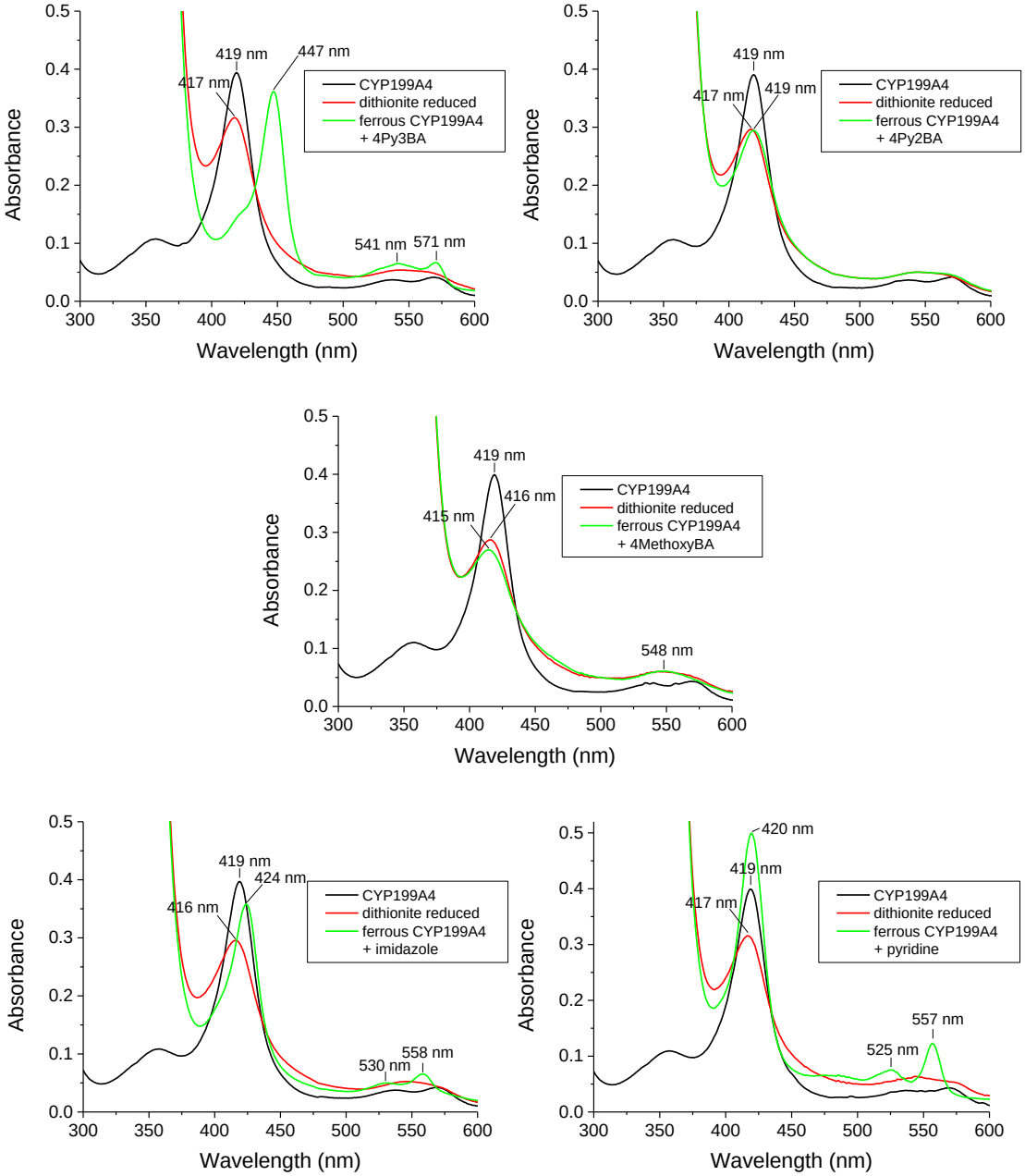

The spectra of ferrous WT CYP199A4 in complex with the type II inhibitors were recorded again, but in this experiment substrate-free CYP199A4 was reduced *prior* to addition of the type II compounds. This experiment was performed in case binding of a nitrogen ligand to the heme may have altered the reduction potential and hindered formation of ferrous iron (see Spectrocelectrochemistry data; Table 1 and Figure S4).

The reduced P450 was subsequently saturated with ligand (≥1 mM) with the exception the ferrous CYP199A4-imidazole and CYP199A4-pyridine complexes, 320 mM imidazole or 250 mM pyridine were added to the reduced P450. The UV-Vis spectrum of the ferric 4-(pyridin-2-yl)benzoic acid-CYP199A4 complex was not altered when dithionite was added to reduce the complex (the Soret band at 422 nm did not shift and no changes were observed in the α/β-band region; Figure S2). This

spectrum is different from that obtained when 4-(pyridin-2-yl)benzoic acid was complexed with CYP199A4 after it had already been reduced. This when combined with the spectroelectrochemical data indicates that 4-(pyridin-2-yl)benzoic acid binding makes chemical reduction with dithionite unfavorable.

Figure S9 Potentiometric titration for HaPux. The inset shows a non-linear least-squares fit of absorbance at 460 nm to a sigmoidal form of the Nernst equation with the number of electrons fixed at 1.

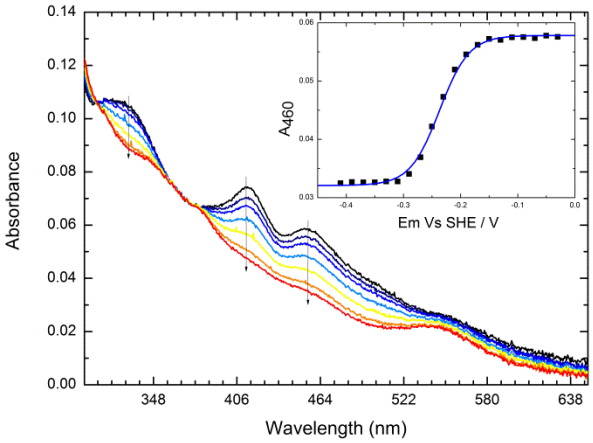

Figure S10 Reduction of **(a)** 4-(pyridin-3-yl)benzoic acid-bound CY199A4 by ferredoxin reductase (HaPuR), ferredoxin (HaPux) and NADH. Reduction of the 4-(pyridin-3-yl)benzoic acid complex shifts the Soret band to 447 nm. **(b)** 4-Pyridin-2-ylbenzoic acid-bound CYP199A4 was not reduced by NADH/HaPux/HaPuR.

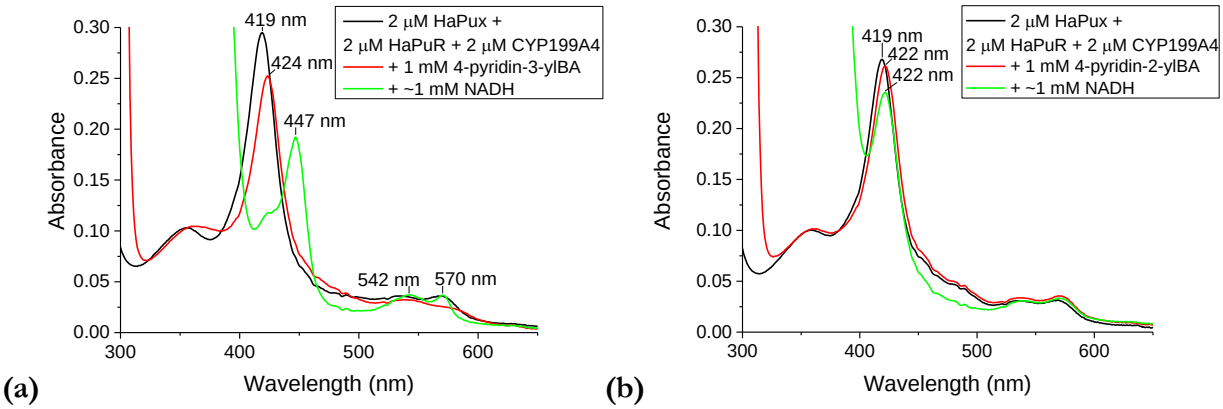

The reaction mixtures contained 2 μM CYP199A4, 2 μM HaPux, 2 μM HaPuR and 1 mM inhibitor. NADH was added to a concentration of ~1 mM. In control reactions omitting HaPuR, the P450 was not reduced (data not shown). When the CYP199A4 complexes with type II ligands were reduced using HaPux/HaPuR/NADH, the complexes with 4-pyridin-3-ylbenzoic acid and 4-pyridin-2-ylbenzoic acid were each left for ~15 min.

Figure S11 Crystals of (**a, b, c**) 4-(pyridin-3-yl)benzoic acid and (**d, e**) 4-(pyridin-2-yl)benzoic acid.

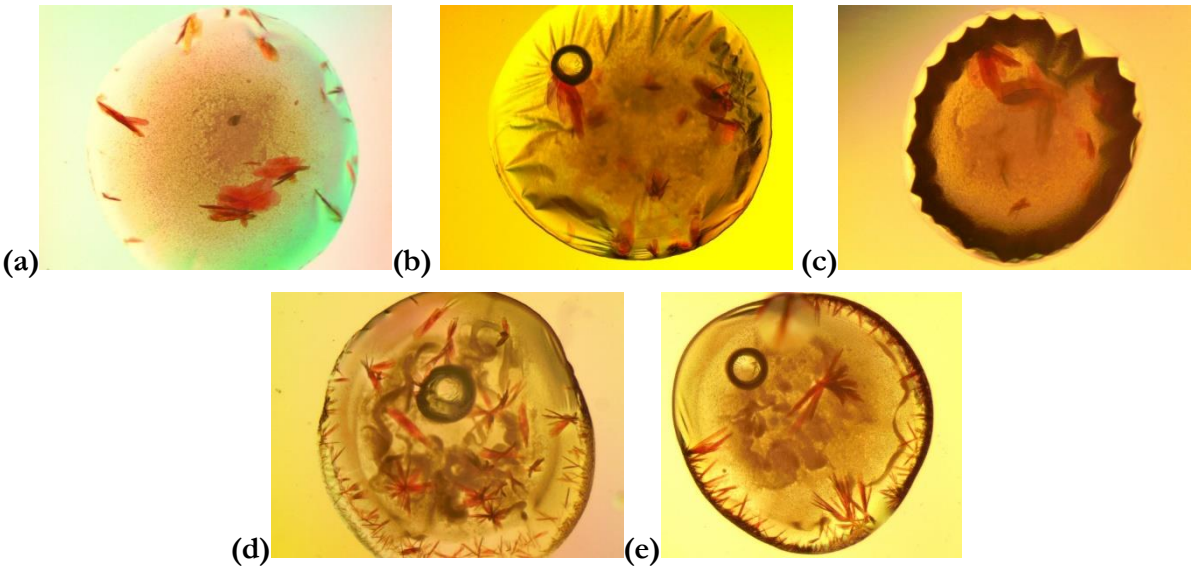

A co-concentration method was used for the pyridine compounds. To dilute protein (~10 μM) was added 4-(pyridin-3-yl)benzoic acid or 4-(pyridin-2-yl)benzoic acid (3 mM) from a 100 mM stock solution in 100% DMSO. The mixture was incubated at 4 ˚C for 2 hours, and the protein-ligand complex was then concentrated to 30-35 mg mL^{-1}. Clusters of red plate-like crystals appeared within half a day to one week.

Figure S12 Superimposition of WT CYP199A4 in complex with type II ligands, **(a)** 4-(pyridin-2-yl)benzoic acid and **(b)** 4-(pyridin-3-yl)benzoic acid, with the structure of 4-methoxybenzoic acid-bound CYP199A4 (PDB: 4DO1). In each image, the Cα trace of 4-methoxybenzoic acid-bound CYP199A4 is in cyan and the heme in green. The Cα trace of CYP199A4 in complex with each type II ligand is shown in yellow (with the heme in magenta). The r.m.s.d. between the Cα atoms is given below each figure (over all 393 pairs of residues).

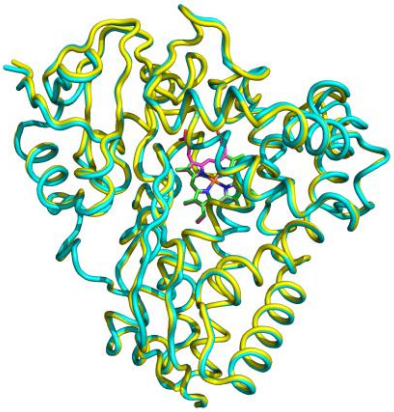

(a) 4-(pyridin-2-yl)benzoic acid (r.m.s.d. = 0.622 Å)

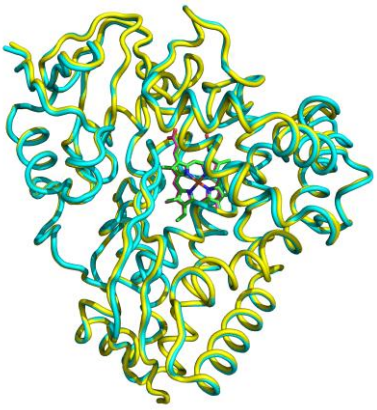

(b) 4-(pyridin-3-yl)benzoic acid (r.m.s.d. = 0.604 Å)

Figure S13 The chloride binding site of WT CYP199A4 in complex with **(a)** 4-(pyridin-2-yl)BA, and **(b)** 4-(pyridin-3-yl)BA. A composite omit map of the chloride anion (purple sphere) is shown as grey mesh contoured at 1.0 σ (1.5 carve).

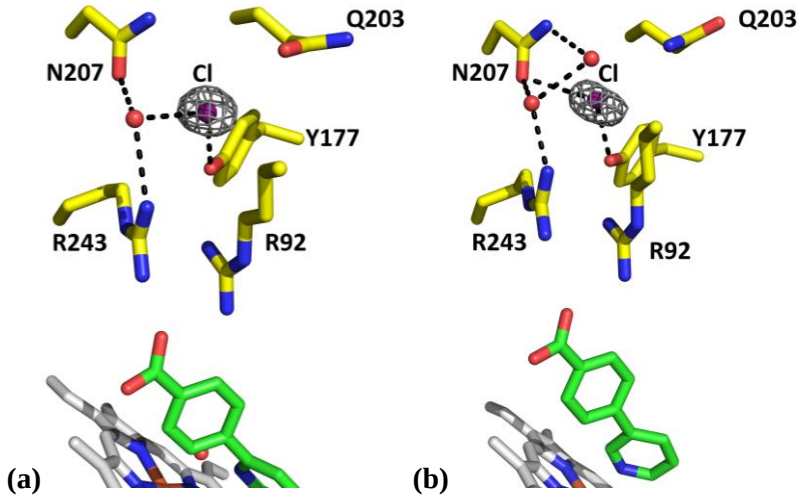

Figure S14 (a) Overlaid structures of 4-(pyridin-3-yl)benzoic acid-bound CYP199A4 (cyan) and 4-methoxybenzoic acid-bound CYP199A4 (yellow, PDB: 4DO1). Distances between equivalent atoms of the benzoic acid moiety are given in Å. In **(b)** the 4-(pyridin-2-yl)benzoic acid structure (cyan) and 4-methoxybenzoic acid structure (yellow) are overlaid. In **(c)** is a view of the active site looking down on the heme. Left: the 4-(pyridin-2-yl)benzoic acid structure (cyan) overlaid with the 4-methoxybenzoic acid structure (yellow). Right: the 4-(pyridin-3-yl)benzoic acid structure (cyan) overlaid with the 4-methoxybenzoic acid structure.

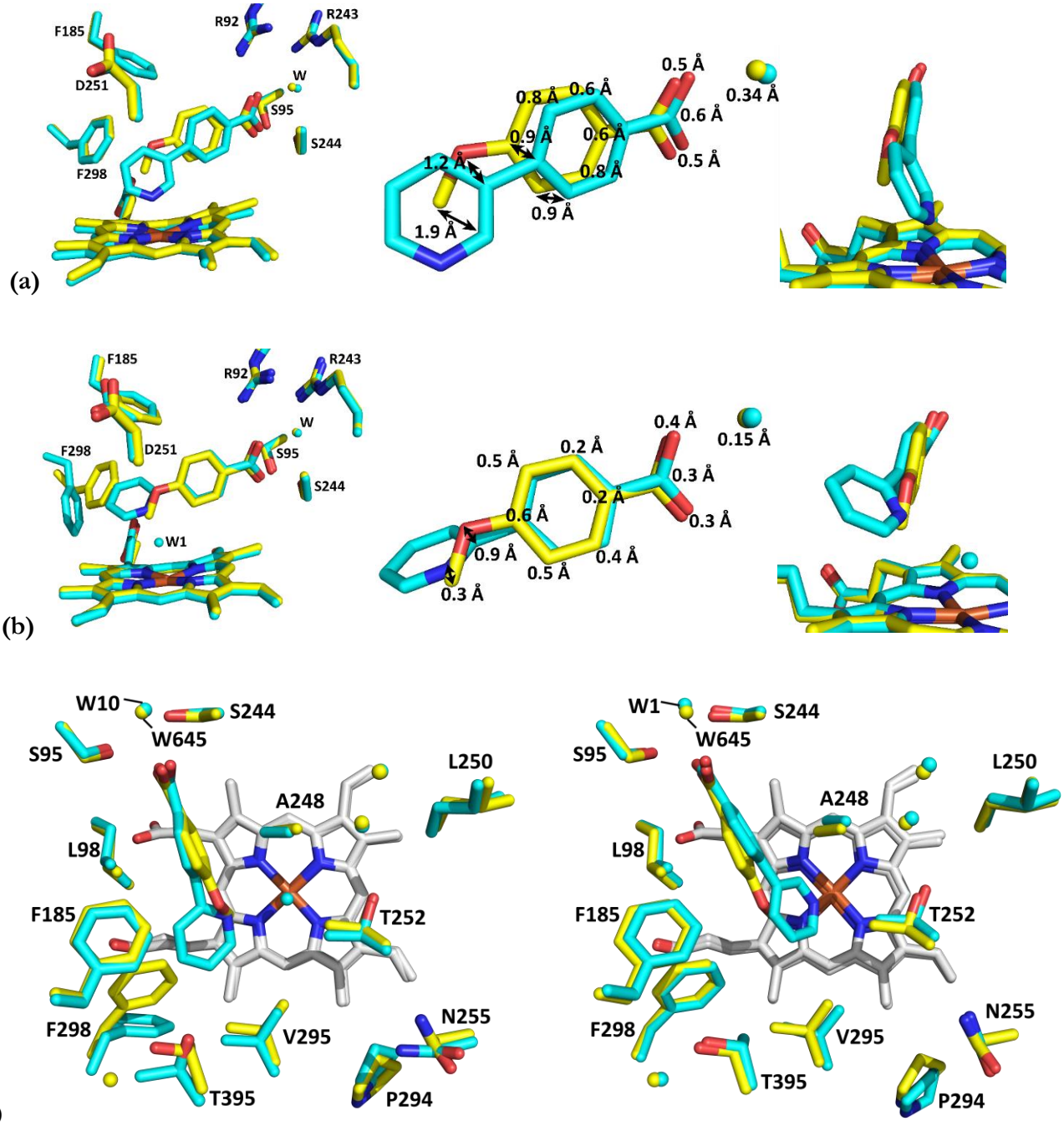

Figure S15 Overlaid structures of 4-(pyridin-3-yl)- (cyan) and 4-(pyridin-2-yl)-benzoic acid-bound CYP199A4 (yellow). An active site water (W1, yellow sphere) is bound to the iron in the 4-(pyridin-2-yl)benzoic acid structure, whereas 4-(pyridin-3-yl)benzoic acid displaces the heme-bound water and the nitrogen coordinates to the iron. F298 shifts to accommodate 4-(pyridin-2-yl)benzoic acid but not when 4-(pyridin-3-yl)benzoic acid binds. The movement of other amino acid residues is also shown. The distances between the atoms of the two pyridinyl benzoic acid isomers are given in Å.

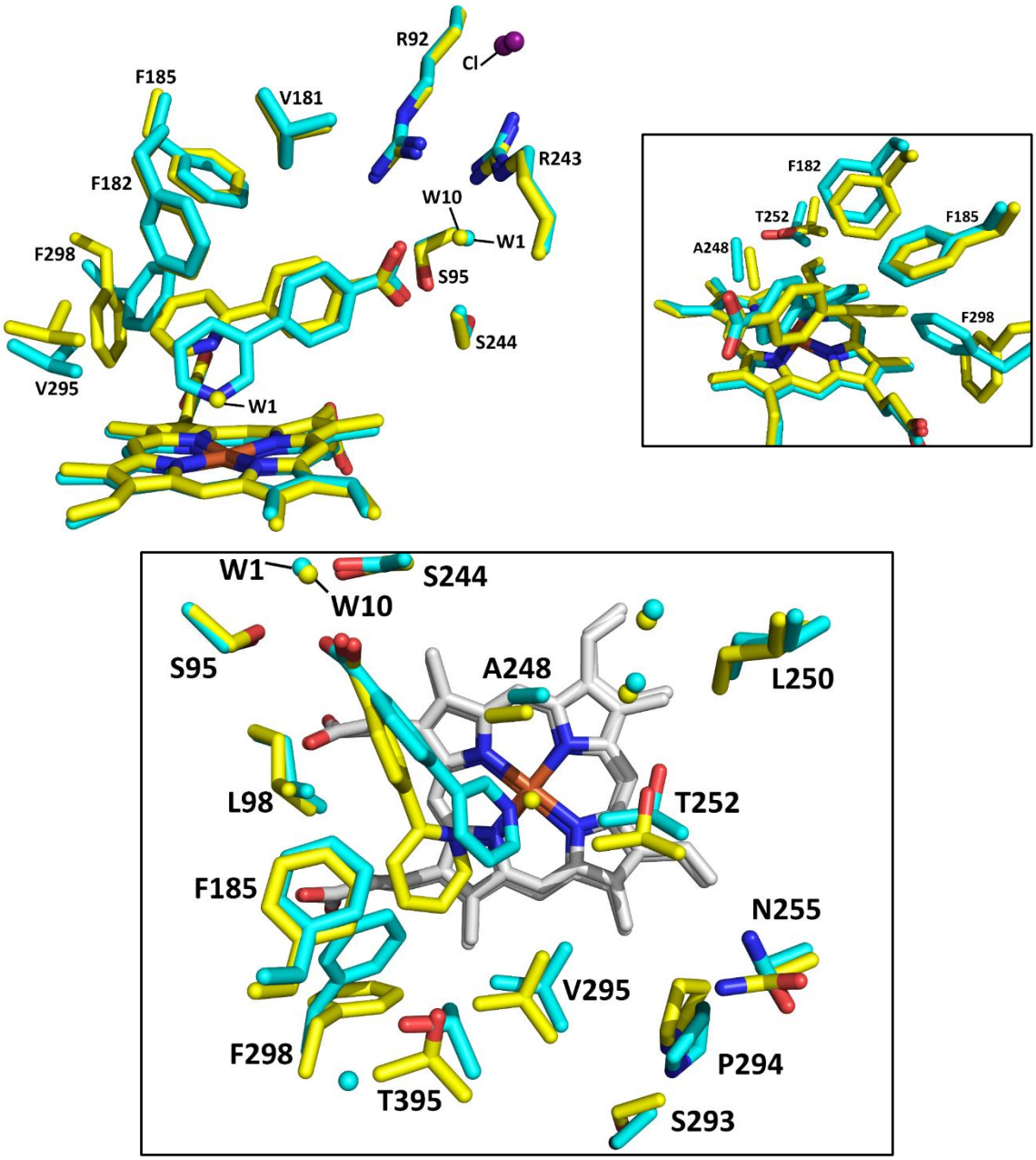

Figure S16 4-(Pyridin-2-yl)benzoic acid displaces the phenyl ring of F298, just as bulky substrates such as 4-ethylthiobenzoic acid have previously been observed to do.[17] In cyan is the 4-ethylthiobenzoic acid structure (5U6U) overlaid with that of 4-(pyridin-2-yl)benzoic acid (yellow).

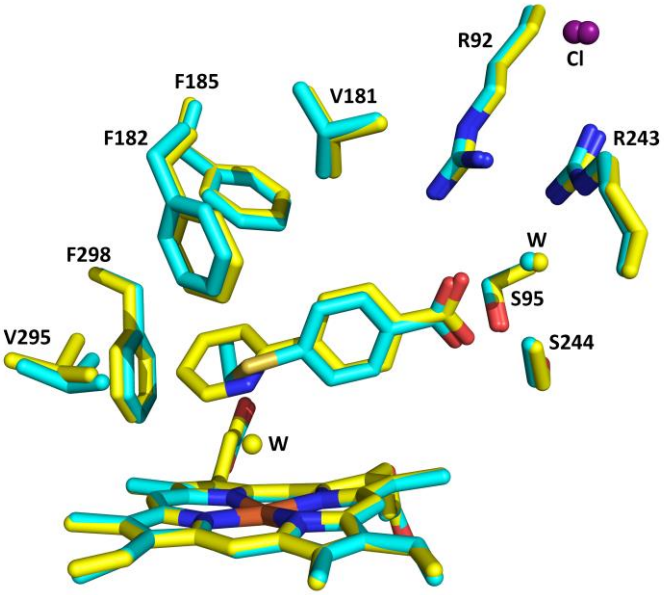

Figure S17 Overlaid structures of 4-(pyridin-2-yl)benzoic acid-bound CYP199A4 (yellow) and 4-ethylbenzoic acid-bound CYP199A4 (cyan; PDB ID: 4EGM). The α-carbon and β-nitrogen of 4-(pyridin-2-yl)benzoic acid are in similar positions to the α- and β-carbons of 4-ethylbenzoic acid.

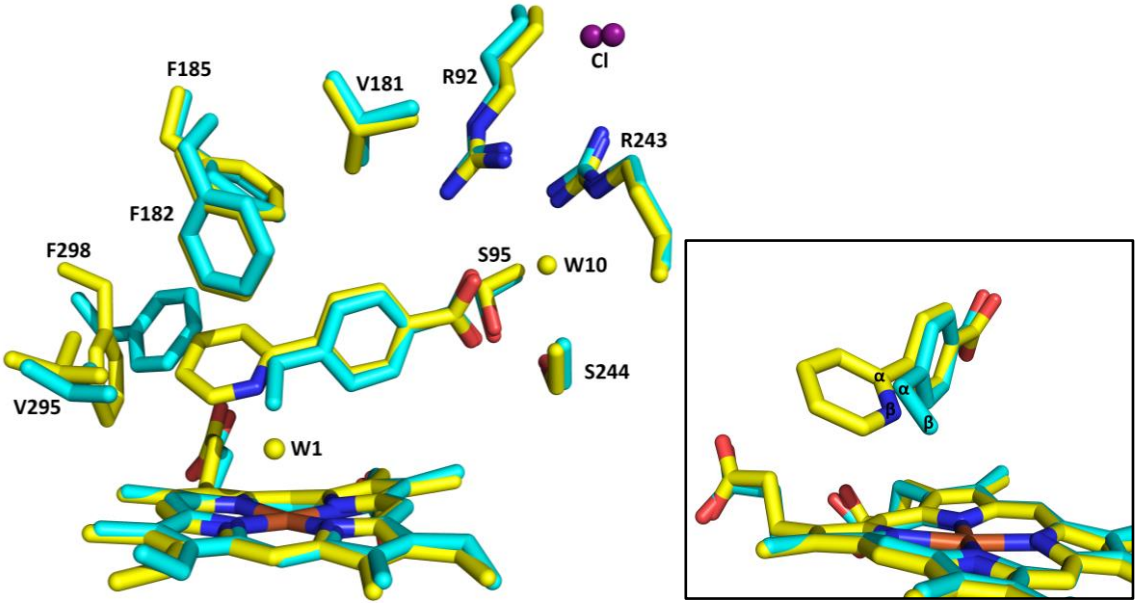

Figure S18 Comparison of the angle of approach of the pyridinyl ring to the heme of 4-(pyridin-3-yl)benzoic acid and 4-(pyridin-2-yl)benzoic acid.

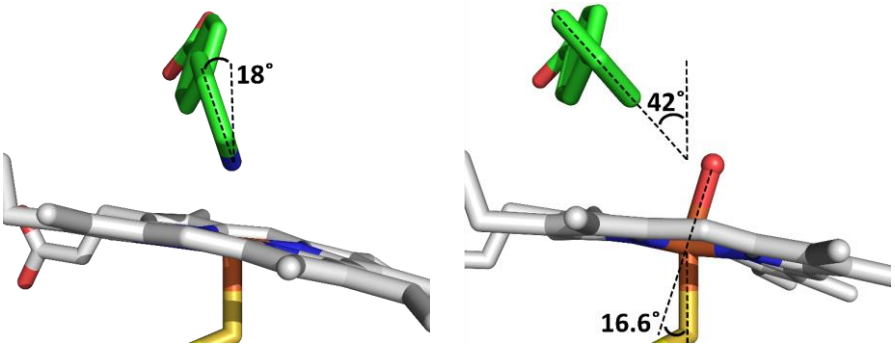

Figure S19 X-band (9.5659 GHz) CW EPR spectrum of substrate-free CYP199A4 recorded at 15 K (power 6.665×10^{-3} mW, modulation amplitude 0.5 mT, modulation frequency 100 kHz). Black – experiment. Blue - simulation comprising a single component. Simulation calculated using principal *g*-values and *g*-strain linewidth broadening. * marks a resonator background signal.

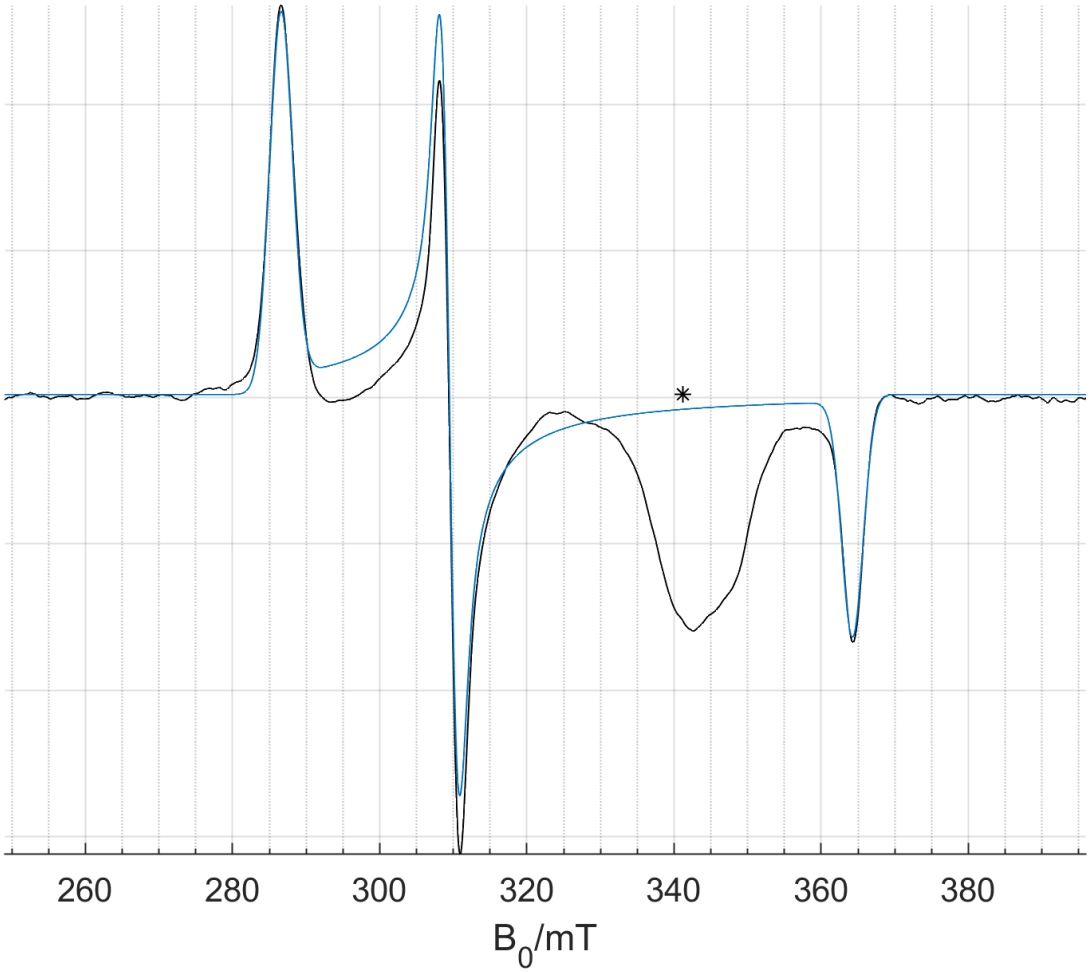

Figure S20 X-band (9.3659 GHz) CW EPR spectrum of CYP199A4 and 4-methoxybenzoic acid recorded at 15 K (power 1.260 mW, modulation amplitude 0.5 mT, modulation frequency 100 kHz). Black – experiment. Sum of simulated components blue, component #1 yellow, #2 purple, #3 green, #4 red. Simulations were calculated using principal *g*-values and *g*-strain linewidth broadening. * marks a resonator background signal.

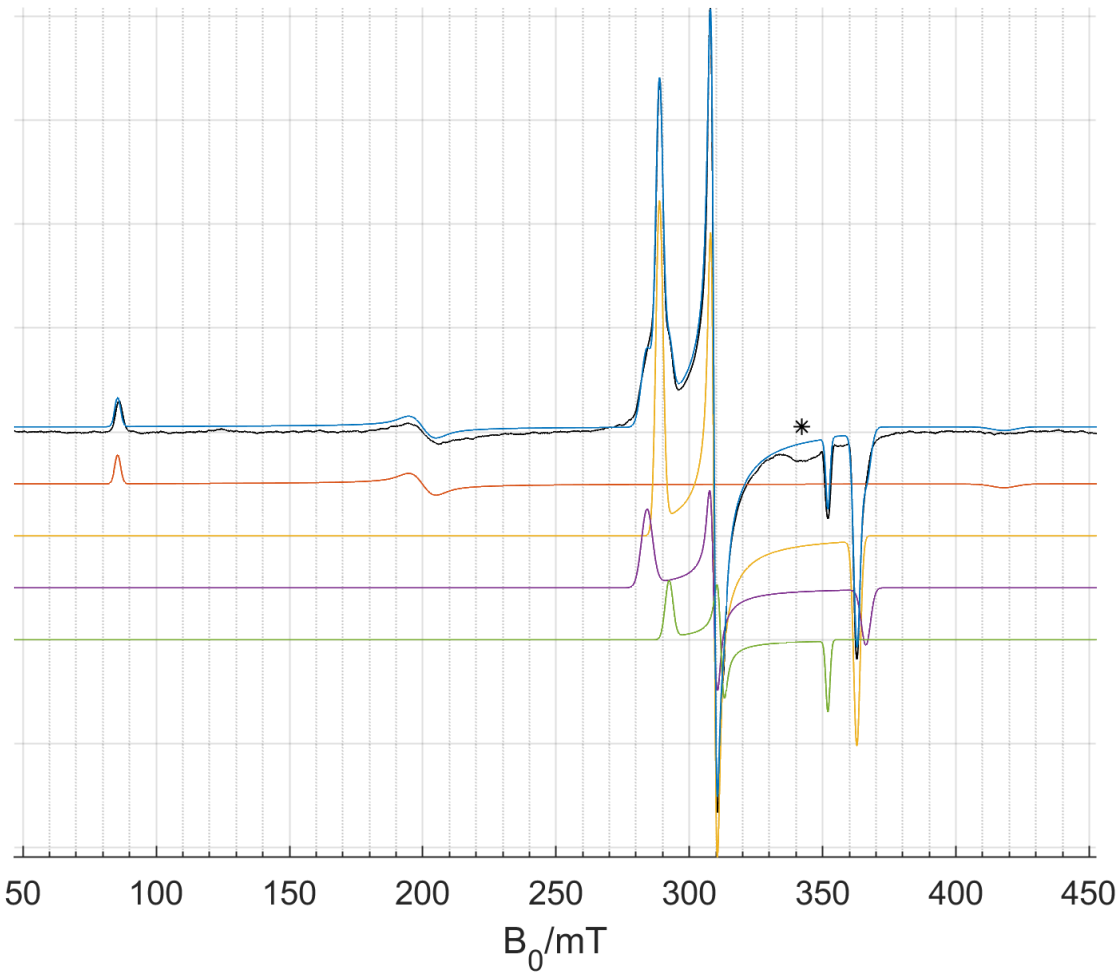

Figure S21 X-band (9.2434 GHz) CW EPR spectrum of CYP199A4 and 4-(pyridin-2-yl)benzoic acid at 15 K (power 6.395×10^{-3} mW, modulation amplitude 0.5 mT, modulation frequency 100 kHz). Black – experiment. Simulation comprising a single component, blue. Simulation calculated using principal *g*-values and *g*-strain linewidth broadening. * marks a resonator background signal.

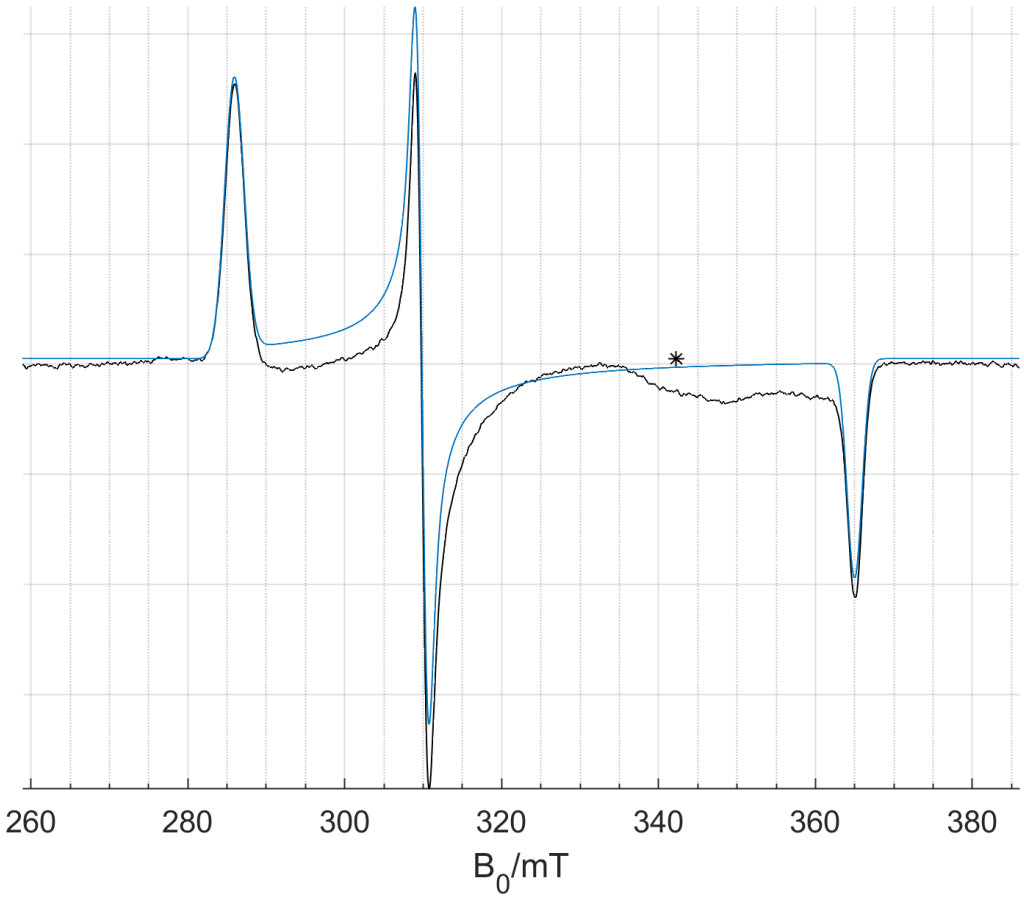

Figure S22 X-band (9.2429 GHz) CW EPR spectrum of CYP199A4 and 4-(pyridin-3-yl)benzoic acid recorded at 15 K (power 7.534×10^{-3} mW, modulation amplitude 0.5 mT, modulation frequency 100 kHz). Black – experiment. Sum of simulated components blue, component #1 red, #2 yellow. Simulations calculated using principal *g*-values and *g*-strain linewidth broadening. * marks a resonator background signal.

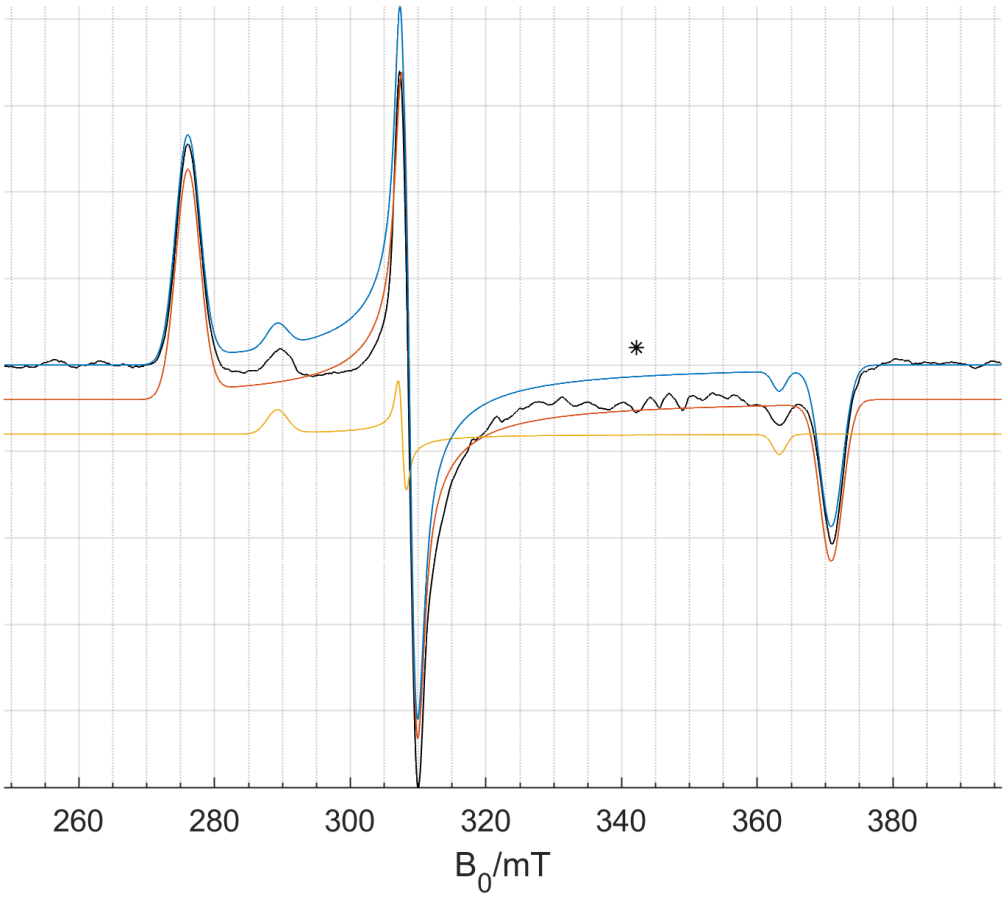

Figure S23 Nitrogen (^{14}N) X-band Mims ENDOR of CYP199A4 with no substrate (NS), 4-methoxybenzoic acid (4MeOBA), 4-(pyridin-2-yl)benzoic acid (4Py2BA), and 4-(pyridin-3-yl)benzoic acid (4Py3BA). Notable is the new signal between 3.5 and 4 MHz upon addition of 4Py3BA, indicating direct coordination of the pyridinyl nitrogen to the Fe^{3+} heme. As expected, ENDOR signals from the directly coordinated ^{14}N nucleus of 4-(pyridin-3-yl)benzoic acid and the pyrrole rings overlap. Data recorded at 12.5 K at the g_y observer position (9.7366 GHz, 308.0 mT) for τ = 82 ns (black) and τ =142 ns (red) showing that τ –dependent blind-spot in the Mims sequence do not affect the analysis of these data.

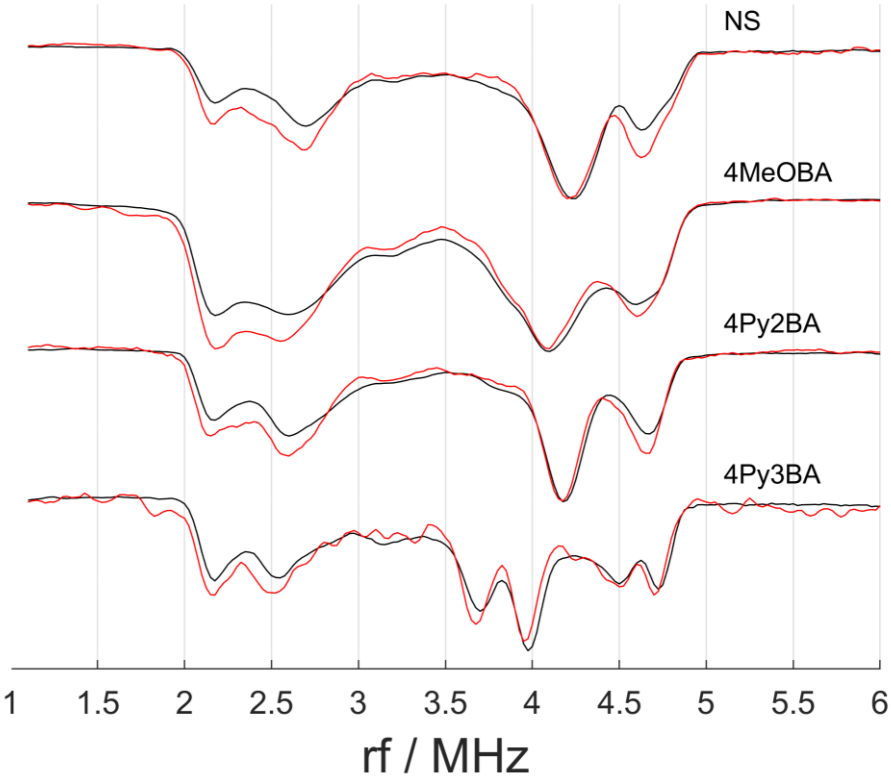

Figure S24 (a) Geometry of five- and six-coordinate ferric heme.[18, 19] In the hexacoordinate, low-spin state, the heme is more or less in the plane of the heme **(b, c)**. High-spin pentacoordinate iron moves below the plane. In the inhibitor-bound CYP199A4 complexes, the iron is approximately in the plane of the heme. **(b, c)** In pentacoordinate, high-spin CYP199A4 complexes, the iron is displaced ~0.3 Å out of the heme plane **(d)**. See Table S8, S9 and S10 for details.

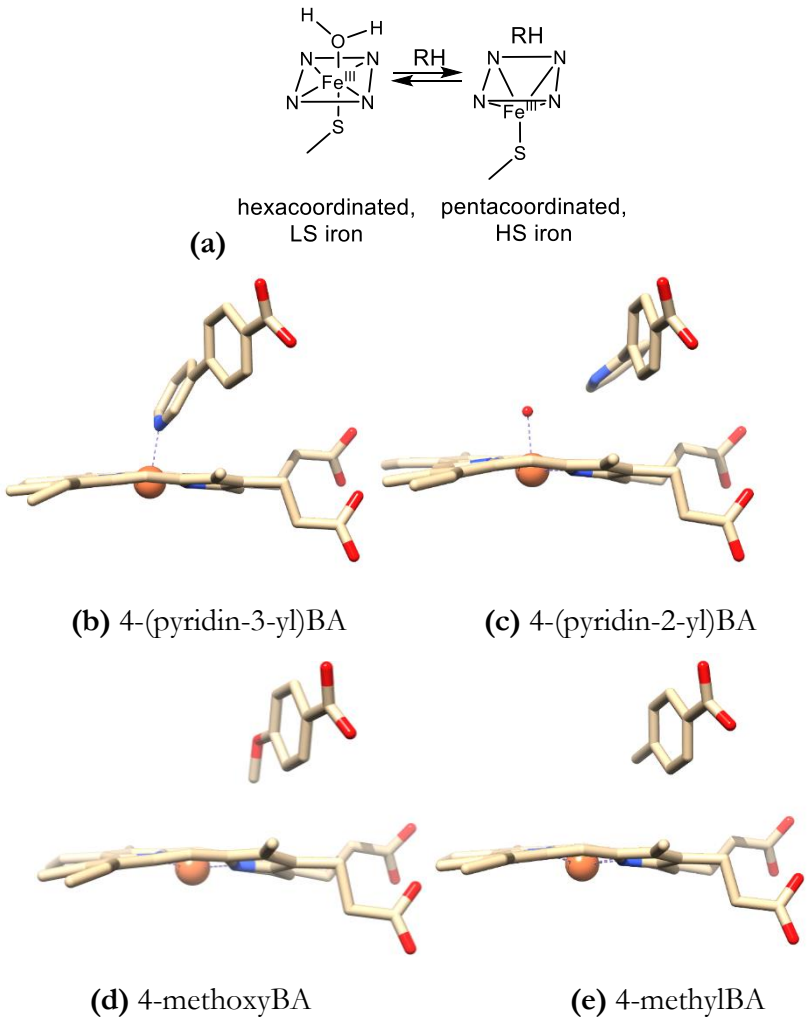

Figure S25 The binding mode of other pyridine substrates to a variety of P450 enzymes as determined by X-ray crystallography. See Table S6 for details.

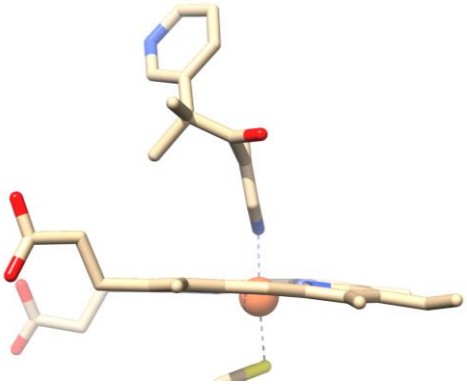

(a) 1PHG

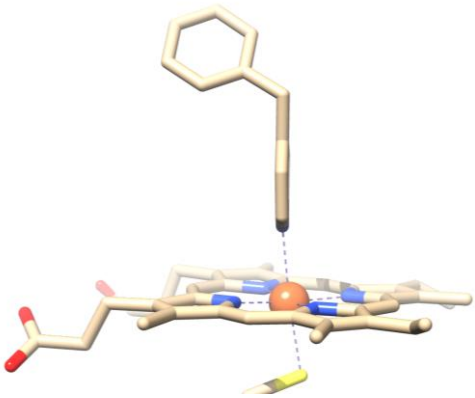

(b) 3QOA

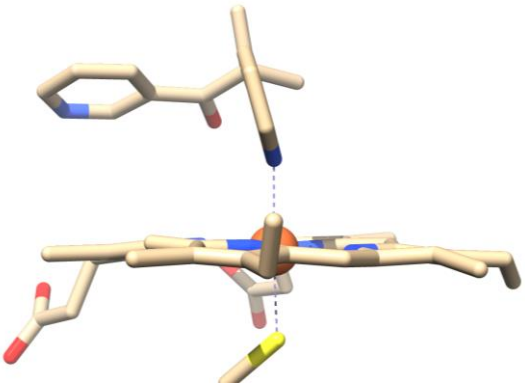

(c) 1W0G

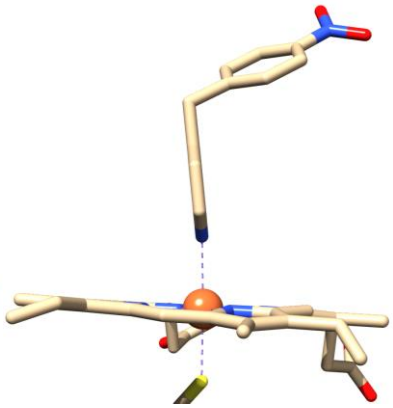

(d) 3QU8

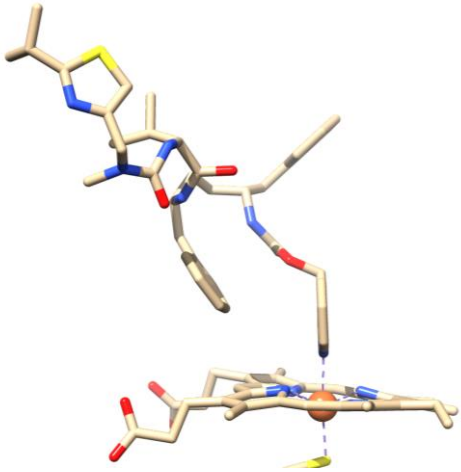

(e) 4I4H

References

[1] Bell, S. G., Tan, A. B., Johnson, E. O., and Wong, L. L. (2010) Selective oxidative demethylation of veratric acid to vanillic acid by CYP199A4 from *Rhodopseudomonas palustris* HaA2, *Mol. Biosyst. 6*, 206-214.

[2] Bell, S. G., Yang, W., Tan, A. B., Zhou, R., Johnson, E. O., Zhang, A., Zhou, W., Rao, Z., and Wong, L. L. (2012) The crystal structures of 4-methoxybenzoate bound CYP199A2 and CYP199A4: structural changes on substrate binding and the identification of an anion binding site, *Dalton Trans. 41*, 8703-8714.

[3] Bell, S. G., Zhou, R., Yang, W., Tan, A. B., Gentleman, A. S., Wong, L. L., and Zhou, W. (2012) Investigation of the substrate range of CYP199A4: modification of the partition between hydroxylation and desaturation activities by substrate and protein engineering, *Chemistry 18*, 16677-16688.

[4] Coleman, T., Chao, R. R., De Voss, J., and Bell, S. G. (2016) The importance of the benzoic acid carboxylate moiety for substrate recognition by CYP199A4 from *Rhodopseudomonas palustris* HaA2, *Biochim. Biophys. Acta Proteins Proteomics 1864*, 667-675.

[5] Maddigan, N. K., and Bell, S. G. (2017) The self-sufficient CYP102 family enzyme, Krac9955, from *Ktedonobacter racemifer* DSM44963 acts as an alkyl- and alkyloxy-benzoic acid hydroxylase, *Arch. Biochem. Biophys. 615*, 15-21.

[6] Williams, J. W., and Morrison, J. F. (1979) The kinetics of reversible tight-binding inhibition, *Methods Enzymol. 63*, 437-467.

[7] Xu, F., Bell, S. G., Rao, Z., and Wong, L. L. (2007) Structure-activity correlations in pentachlorobenzene oxidation by engineered cytochrome P450cam, *Protein Eng. Des. Sel. 20*, 473-480.

[8] Coleman, T., Chao, R. R., Bruning, J. B., De Voss, J. J., and Bell, S. G. (2015) CYP199A4 catalyses the efficient demethylation and demethenylation of *para*-substituted benzoic acid derivatives, *RSC Adv. 5*, 52007-52018.

[9] Markley, J. L., Bax, A., Arata, Y., Hilbers, C. W., Kaptein, R., Sykes, B. D., Wright, P. E., and Wüthrich, K. (1998) Recommendations for the presentation of NMR structures of proteins and nucleic acids – IUPAC-IUBMB-IUPAB Inter-Union Task Group on the Standardization of Data Bases of Protein and Nucleic Acid Structures Determined by NMR Spectroscopy, *J. Biomol. NMR 12*, 1-23.

[10] Sevrioukova, I. F., and Poulos, T. L. (2013) Pyridine-Substituted Desoxyritonavir Is a More Potent Inhibitor of Cytochrome P450 3A4 than Ritonavir, *J. Med. Chem. 56*, 3733-3741.

[11] Shah, M. B., Pascual, J., Zhang, Q., Stout, C. D., and Halpert, J. R. (2011) Structures of Cytochrome P450 2B6 Bound to 4-Benzylpyridine and 4-(4-Nitrobenzyl)pyridine: Insight into Inhibitor Binding and Rearrangement of Active Site Side Chains, *Mol. Pharmacol. 80*, 1047-1055.

[12] Williams, P. A., Cosme, J., Vinković, D. M., Ward, A., Angove, H. C., Day, P. J., Vonrhein, C., Tickle, I. J., and Jhoti, H. (2004) Crystal Structures of Human Cytochrome P450 3A4 Bound to Metyrapone and Progesterone, *Science 305*, 683-686.

[13] Poulos, T. L., and Howard, A. J. (1987) Crystal structures of metyrapone- and phenylimidazole-inhibited complexes of cytochrome P-450cam, *Biochemistry 26*, 8165-8174.

[14] Dick, S. (1998) Crystal structure of tris(2,2'-bipyridine)iron(II) bis(hexafluorophosphate), (C10H8N2)3Fe(PF6)2, In *Zeitschrift für Kristallographie - New Crystal Structures*, p 370.

[15] Dawson, J. H., Andersson, L. A., and Sono, M. (1982) Spectroscopic investigations of ferric cytochrome P-450-CAM ligand complexes. Identification of the ligand *trans* to cysteinate in the native enzyme, *J. Biol. Chem. 257*, 3606-3617.

[16] Dawson, J. H., Andersson, L. A., and Sono, M. (1983) The diverse spectroscopic properties of ferrous cytochrome P-450-CAM ligand complexes, *J. Biol. Chem. 258*, 13637-13645.

[17] Coleman, T., Wong, S. H., Podgorski, M. N., Bruning, J. B., De Voss, J. J., and Bell, S. G. (2018) Cytochrome P450 CYP199A4 from *Rhodopseudomonas palustris* catalyzes heteroatom dealkylations, sulfoxidation, and amide and cyclic hemiacetal formation, *ACS Catal. 8*, 5915-5927.

[18] Shaik, S., Kumar, D., de Visser, S. P., Altun, A., and Thiel, W. (2005) Theoretical Perspective on the Structure and Mechanism of Cytochrome P450 Enzymes, *Chem. Rev. 105*, 2279-2328.

[19] Conner, K. P., Woods, C. M., and Atkins, W. M. (2011) Interactions of cytochrome P450s with their ligands, *Arch. Biochem. Biophys. 507*, 56-65.